Authors:
Dr. Lilian A. Dove, dove@brown.edu
Prof. Mara A. Freilich, mara_freilich@brown.edu
Prof. Lia Siegelman, lsiegelman@ucsd.edu
Prof. Baylor Fox-Kemper, baylor@brown.edu
Dr. Paul Hall, paul_hall@brown.edu

Pycnocline Stratification Shapes Submesoscale Vertical Tracer Transport

Lilian A. Dove[a,b] , Mara A. Freilich[a] , Lia Siegelman[c] , Baylor Fox-Kemper[a] , Paul Hall[a]

[a] *Brown University, Providence, Rhode Island, USA,* [b] *Cooperative Programs for the Advancement of Earth System Science, University Corporation for Atmospheric Research, Boulder, Colorado, USA,* [c] *Scripps Institution of Oceanography, La Jolla, California, USA*

Corresponding author: Lily Dove, dove@brown.edu

ABSTRACT: Pycnocline stratification is increasing across multiple ocean basins due to a warming surface ocean and increasing sea ice melt. Pycnocline stratification plays a leading order role in tracer transport, shaping capacity for heat and carbon uptake, making it a key parameter of interest on timescales ranging from paleoclimate to plankton blooms. Part of the challenge in assessing the role of pycnocline stratification in global models is the two-way connection between physical processes at the (sub)mesoscale and stratification with important implications for tracer subduction. Using a suite of numerical simulations of an idealized front, we find that the strength of pycnocline stratification influences the formation and evolution of submesoscale structure and the resulting tracer transport. The impact of changing stratification on tracer flux strongly depends on whether frontal strength is also changed correspondingly by holding the isopycnal slope fixed. When a constant isopycnal slope is initialized, tracers get efficiently transferred across the base of the mixed layer and get trapped in anticyclonic submesoscale vortices below the mixed layer. This leads to tracer concentrations below the mixed layer and fluxes through it to be stronger under decreased stratification conditions. In contrast, when frontal lateral buoyancy gradient is held fixed while stratification changes, the vertical flux of tracers and the concentrations at depth stay constant across all examined stratification conditions. Understanding the relationship between pycnocline stratification and fine-scale physical motions is necessary to diagnose and predict trends in carbon uptake and storage, particularly in the Southern Ocean.

SIGNIFICANCE STATEMENT: Due to climate change, the ocean is warming. As a result, the stratification, or vertical layering of density, in the ocean is increasing. We use a numerical model to investigate how this increasing stratification impacts motions that are approximately 0.1-10 km in width. These motions are known to play a vital role in transporting properties from the ocean surface (*e.g.* carbon stored in phytoplankton) into the interior ocean. Although these processes may seem separate due to large differences in scale (ocean basin versus 1 km), the small-scale motions are fueled by the large-scale background conditions. We find that there is a relationship between background stratification and transport between the surface and interior ocean; in particular, when the stratification is decreased, there is enhanced downward movement of surface properties. However, despite an *a priori* expectation that increasing stratification may reduce the ability of the ocean to take up and store surface ocean properties, we demonstrate that uptake via these processes may "plateau" and there may not necessarily be a reduction in the drawdown via small-scale motions.

1. Introduction

In an averaged view of a vertical column of the ocean, the surface mixed layer and the deep ocean are separated by a region of enhanced density stratification. The strength of this stratification has implications for the climate, as enhanced stratification can result in reduced exchange of oceanic tracers between the surface and interior ocean with impacts on biological productivity (Behrenfeld et al. 2006), air-sea gas exchange (Sallée et al. 2012), and ocean heat and carbon uptake and storage (Newsom et al. 2023; Bourgeois et al. 2022). Investigations using numerical models and observations have found that stratification in the surface ocean has increased globally by 5.3%-8.9% since 1960 (Li et al. 2020; Sallée et al. 2021; Roch et al. 2023). The relationship between subsurface stratification and surface buoyancy forcing is complex (Somavilla et al. 2017), but overall, increasing pycnocline stratification is associated with surface warming and freshening at high latitudes (Yamaguchi and Suga 2019) and mid to tropical latitudes (Luyten et al. 1983), as well as through wind-driven processes responding to freshening at midlatitudes (Fedorov et al. 2004). Stratification is a major uncertainty in climate models, with significant impact on future projections of oceanic heat uptake and storage (Bourgeois et al. 2022). Significantly, the impact of pycnocline stratification on smaller, surface-forced physical scales and mechanisms remains unattributed, and these ubiquitous dynamics are not captured in climate models with insufficient resolution.

Density fronts in the global ocean play a fundamental role in shaping subsurface ocean properties through subduction of surface ocean properties along sloping isopycnals. Subduction occurs through both mesoscale stirring processes, submesoscale vertical advection, and the combination of these processes (Freilich et al. 2024; Cao et al. 2024). Motions in the ocean surface boundary layer can significantly alter upper-ocean stratification and exchange between the mixed layer and the thermocline by frontal circulations (Klein and Lapeyre 2009) or mixing and turbulent entrainment (Smith et al. 2016) with downstream implications for ocean biogeochemistry (Mahadevan 2016; Lévy et al. 2018; McGillicuddy 2016). Mesoscale eddies shed off density fronts and work to restratify the front. Sourcing energy from the mesoscale strain field, submesoscale fronts are traditionally Rossby number and Richardson number of $O(1)$, dynamical regimes where rotation and inertial forces are of comparable importance (McWilliams 2019). Submesoscale motions are associated with elevated vertical velocities $O(100\text{ m day}^{-1}$; Su et al. (2018)) that can penetrate up to 100 m below the base of mixed layer (Siegelman et al. 2020; Siegelman 2020). These vertical circulations can transport surface waters below the base of the mixed layer, sequestering surface-enhanced organic carbon through the downwelling pathway (Boyd et al. 2019; Ruiz et al. 2009). In addition, nutrients that have elevated concentrations at depth can be entrained into the mixed layer through the restratification process (Brannigan 2016; Luo and Callies 2023). Submesoscale-resolving observations from the last decade have confirmed predictions by numerical models (Rosso et al. 2015; Balwada et al. 2018) that submesoscale structure is ubiquitous across the global ocean and plays a key role in setting subsurface tracer distributions (Freilich and Mahadevan 2021), particularly in energetically enhanced regions of the global ocean such as the Southern Ocean (Dove et al. 2021).

The relationship between pycnocline stratification and mesoscale and submesoscale motions can be explored with a thought experiment. If pycnocline stratification (N^2) at a front increases without a requisite strengthening of the horizontal density gradient (M^2), the isopycnal slope (M^2/N^2) of the front will decrease, reducing the available potential energy for mesoscale instability and the submesoscale motions fueled by mesoscale strain (Rosso et al. 2015). However, if the horizontal density gradient also increases, the isopycnal slope can remain constant. A real-world example of a constant isopycnal slope under changing conditions is the major fronts of the Antarctic Circumpolar Current (ACC). A poleward shift and intensification of westerly winds (Meredith et al. 2012; Downes et al. 2011) and the north-south asymmetry of warming across the Southern Ocean (Shi et al. 2021) both correlate with accelerations of the zonal flow. The "eddy saturation" hypothesis suggests that despite these basin-wide changes, the additional energy is imparted to mesoscale eddies (Morrison and Hogg 2013; Munday et al. 2013; Constantinou and Hogg 2019; Hogg et al. 2015). The eddy kinetic energy across the Southern Ocean is increasing, suggesting enhanced mesoscale eddy activity (Martínez-Moreno et al. 2021; Zhang et al. 2021) and the isopycnal slope across the ACC is observed to be relatively constant (Böning et al. 2008).

Increased pycnocline stratification may reduce the capacity of mixed layer processes to source energy from greater depths, as the wintertime mixed layer depth (MLD) tends to shallow with reduced stratification. The wintertime MLD depth has long been considered critical for setting potential primary productivity and nutrient entrainment (Sverdrup 1953). The relationship between stratification and MLD is of particular interest to the polar community, as the two poles are experiencing opposite responses. In the Arctic, there is decreasing stratification due to reduced freshwater inputs, resulting in a deepening MLD and enhanced vertical mixing (Hordoir et al. 2022). In the Southern Ocean, despite increasing stratification due to surface warming and sea ice melt, the MLD is deepening, attributed to increasingly strong westerly winds (Sallée et al. 2021). Increased available potential energy resulting from deepening MLDs can provide the energy necessary for mesoscale instability and fuel submesoscale motions.

Here, we present output from a submesoscale-resolving process model with a density front to investigate the relationship between initial pycnocline stratification and the vertical transport of oceanic tracers. We demonstrate that the physical response to stratification changes, and therefore the tracer transport, is dependent on the response of the isopycnal slope to changing stratification. Tracers subducted from the mixed layer are captured in anticyclonic submesoscale coherent vortices. The number of these features are enhanced in decreased stratification conditions, particularly in conditions where the large-scale cross-front buoyancy gradient adapts to changing stratification resulting in a constant isopycnal slope. However, increased stratification does not necessarily result in decreased tracer at depth. This is in contrast to previous research which suggests that increasing pycnocline stratification will reduce submesoscale activity and therefore tracer subduction.

2. Data and Methods

Model setup

A series of numerical experiments were carried out using the Massachusetts Institute of Technology general circulation model (MITgcm; Marshall et al. (1997)) (Figure 1). The model setup consists of a square channel of size 512 km by 512 km by 3000 m on a β-plane (centered at 50°S) and flat bottom topography. The southern edge is blocked by a vertical wall and the northern edge linearly restores to a set temperature profile. The surface has an additional buoyancy forcing of -50 W m^{-2} (where negative values represent a loss of heat from the ocean to the atmosphere) and is forced by a zonal atmospheric jet centered at the middle of the domain. The atmospheric jet causes Ekman pumping to the north and Ekman suction to the south. There is no seasonal or tidal forcing, and buoyancy is controlled solely by temperature as an active tracer. The numerical viscosity is set by the modified 2D Leith viscosity (Fox-Kemper and Menemenlis 2008) and in the vertical direction, the K-Profile Parameterization (KPP) is used for boundary layer turbulent mixing. The vertical grid is the same as used in the LLC4320 simulations, with spacing of ≈1 m near the surface and increased spacing with depth (Rocha et al. 2016). We define an isolated front using an initial temperature relationship (Equation 1) that is in thermal wind balance with the along-front zonal wind velocity.

$$T_0 = (T_N - T_S)\tanh\left(\frac{y - \frac{L_y + y_{meander}}{2}}{L_f} + 1\right) + T_S \tag{1}$$

$$y_{meander} = 5\sin\left(\frac{2\pi x}{L_y}\right) \tag{2}$$

where the T_0 is initial temperature, T_N is the temperature at the northern boundary, T_S is the temperature at the southern boundary, L_f is the frontal width, and L_y is the width of the domain (Stamper et al. 2018). To jump start eddy formation, a small (5 kilometer amplitude) meander is added to the front, defined by $y_{meander}$. The initial mixed layer depth (MLD) is set at 117 meters for all simulations, with the MLD calculated by a potential density difference criterion of 0.03 kg m^{-3} from the potential density at 10 meters (Montégut et al. 2004; Treguier et al. 2023). Initial spin-up runs last for 220 days, reaching approximately steady state conditions around day 170, with some variance between initial conditions.

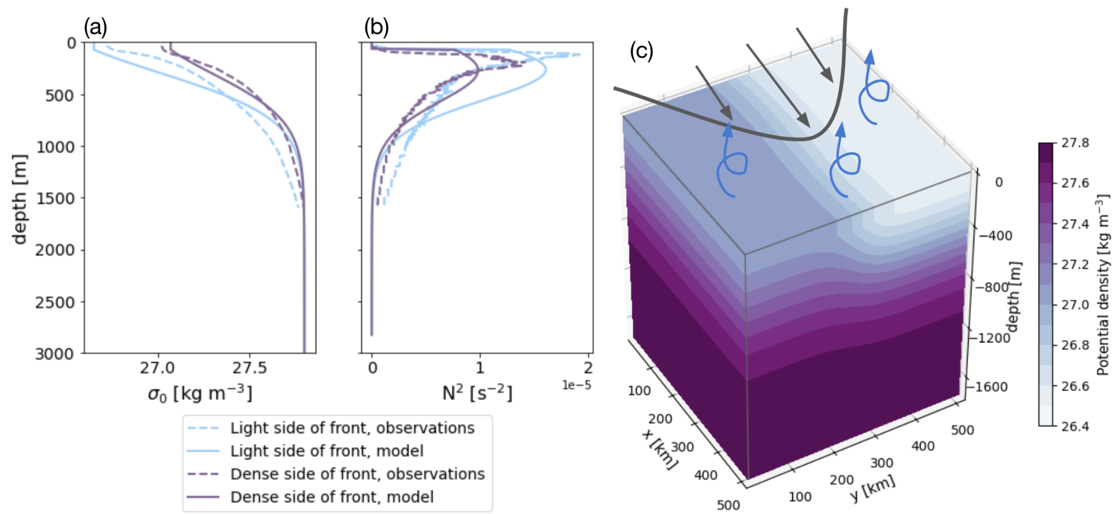

Fig. 1. Setup of the MITgcm. Observations from Argo floats upstream of Kerguelen plateau compared to initial conditions of the baseline simulation of (a) potential density (σ_0, kg m^{-3}) and (b) vertical stratification (N^2, s^{-2}). (c) Schematic of the simulation setup, plotting potential density. Gray line and arrows indicates the relative magnitude and direction of wind stress. Blue arrows represent constant surface cooling of -50 W m^{-2}.

The "baseline" conditions are set to mimic potential density across the Antarctic Polar Front in the ACC, informed by data from Argo float profiles upstream of the Kerguelen plateau (40 to 60°E, 40 to 50°S; Figure 1a,b). It should be noted that salinity plays a significant role in setting the density, and therefore stratification, distribution of the Southern Ocean, particularly south of the Polar Front (Stewart and Haine 2016). However, to maintain ease of comparison, we employ only temperature as an active tracer with a constant salinity of 35 g kg^{-1} across the whole domain. The surface buoyancy forcing mimics forcing experienced at this latitude in austral springtime.

Experiment description

Different pycnocline stratification conditions are tested (Figure 2), ranging from an initial maximum N^2 = 1.09 e^{-5} s^{-2} to N^2 = 2.07 e^{-5} s^{-2}. Under cases where the isopycnal slope (M^2/N^2) is held constant at Γ = 4 e^{-3} at the base of the mixed layer, the initial, large-scale lateral buoyancy gradient, M^2, is modified (Figure 2a). Where the changing isopycnal slope is considered, the surface M^2 is held constant (Figure 2b). The resulting simulations are referred to as "increased stratification" and "decreased stratification" conditions. In all constant slope conditions, the initial isopycnal slope is the same across all runs (Figure 2c,d,f). In changing slope conditions, the initial slope varies across runs (Figure 2c,e,g), where increased vertical stratification leads to a reduced isopycnal slope and decreased vertical stratification leads to an increased isopycnal slope. The terms "constant" and "changing" only apply to the initial conditions of the simulations; no nudging or forcing is used to maintain or change the slope. However, we use this terminology throughout to differentiate the two cases.

Tracers are seeded across the full domain at 5 meters depth upon the model reaching a steady state conversion of available potential energy to kinetic energy (Figure 3). The tracers were seeded evenly across the full domain with a value of 1 mol m^{-3}. For all cases, tracers were released on day 170 after initialization, with averages of tracer concentrations and fluxes considered between days 199-219.

Non-dimensional numbers

The Rossby number (Ro) is used to diagnose scales of motion, where processes that are near 0 defined as geostrophic, and Ro $O(1)$ being a typical definition of the submesoscale, particularly in the surface ocean. Using the horizontal velocities (u, v), Coriolis parameter (f), and the lateral and vertical buoyancy gradient scales (M^2, N^2), and the vertical shear (S), the dimensionless Rossby number can be written, and approximately scaled under geostrophy, as,

$$Ro = \zeta f^{-1} = \left(\frac{\partial u}{\partial y} - \frac{\partial v}{\partial x}\right) f^{-1} \sim \frac{M^2 H}{f^2 L}. \tag{3}$$

The gradient Richardson number (Ri_g) characterizes the stability of a flow in the presence of a density gradient. As the balance between potential energy associated the vertical buoyancy gradient to the kinetic energy associated with vertical shear, a $Ri_g < 1$ indicates the flow is potentially unstable and allowing for the development of turbulence. The Richardson number also scales under geostrophy with the lateral and vertical buoyancy gradients.

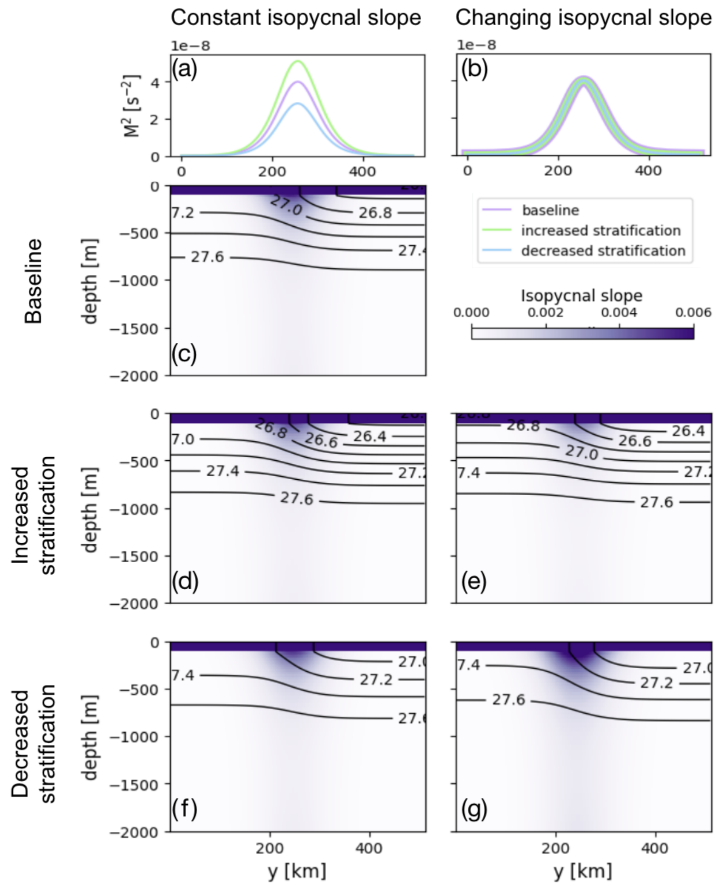

FIG. 2. Initial conditions for the MITgcm. Horizontal density gradient (M^2, s^{-2}) for the (a) constant isopycnal slope and (b) changing isopycnal slope conditions. In (b), the lines are thickened to show how the the three conditions are "stacked" on top of each other. Isopycnal slope (M^2/N^2) for the (c) baseline conditions, increased stratification conditions for (d) constant slope and (e) changing slope, and decreased stratification conditions for (f) constant slope and (g) changing slope.

$$Ri_g = N^2 S^{-2} = \frac{\partial b}{\partial z}\left(\frac{\partial \bar{u}_h}{\partial z}\right)^{-2} \sim \frac{N^2 f^2}{M^4}. \tag{4}$$

Luo and Callies (2023) finds that the ratio of the Richardson numbers between the mixed layer and the pycnocline is a key metric for transport by submesoscales into the ocean interior. We do not revisit this hypothesis here, but instead examine two cases where the Richardson number of the mixed layer is altered in different directions. In one direction, where the isopycnal slope is held constant, we find results that seemingly disagree with those of Luo and Callies (2023), although it

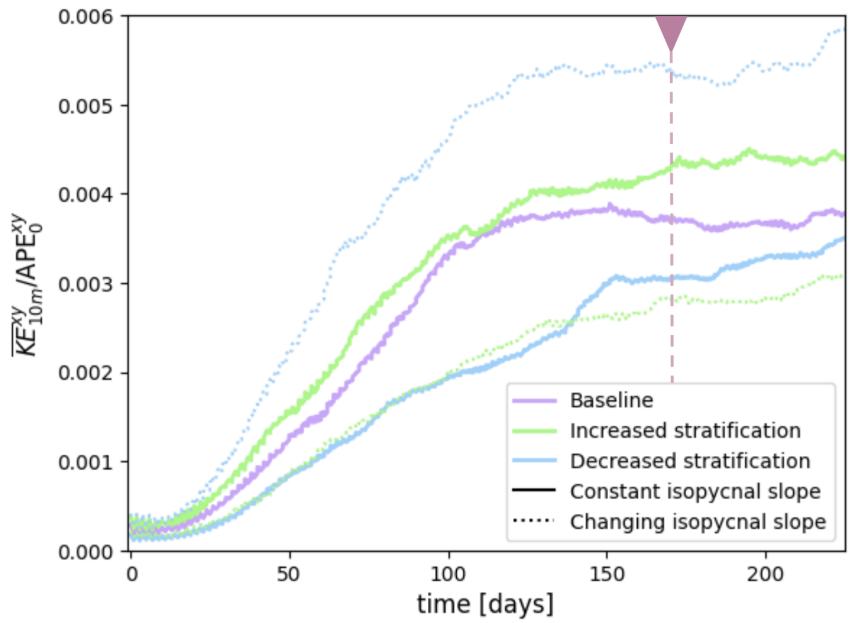

FIG. 3. Evolution of surface kinetic energy in the model simulations. Kinetic energy at 10 m depth averaged over the full model domain is normalized by the initial available potential energy averaged over the full model domain. Solid lines are runs with constant isopycnal slope conditions while dashed lines are runs with changing isopycnal slope conditions. Pink triangle and line denote the time when tracers were released.

is important to note that there are distinct methodology and metrics distinctions between our study and theirs.

The isopycnal slope (Γ) is the final dimensionless parameter of note. Its magnitude is:

$$\Gamma = \left| \frac{M^2}{N^2} \right| . \tag{5}$$

Constant isopycnal slope will be a key option sometimes taken for the experimental design here. It is also important to note that the (Fox-Kemper et al. 2008) explicitly depends on M^2, but not on N^2 in the mixed layer (it does so only indirectly through mixed layer depth), so the restratification by mixed layer eddies within the mixed layer is expected to strongly depend on whether M^2 varies across runs. This occurs in these experiments *only* under the constant isopycnal slope simulations.

3. Results

Frontal subsurface evolution

The source of energy for the evolving mesoscale and submesoscale field is the available potential energy from the density front. The evolution of the front with time is investigated by calculating $\overline{b^{xz}}$ - b_0^{xz}, or the difference between the average buoyancy the along-front and vertical directions and the initial buoyancy conditions. Larger magnitudes of $\overline{b^{xz}}$ - b_0^{xz} suggest greater differences in buoyancy from the initial condition. In all cases, the north (light) side of the front becomes less buoyant while the south (dense) side of the front becomes more buoyant, the expected response for a front that is restratifying through overturning. The reduced buoyancy across the whole domain (light blue) at all timesteps is a result of the surface cooling initial condition.

In the cases where the isopycnal slope of the front is held constant (Figure 4a,b,d), with increased stratification, a large cross-front lateral buoyancy gradient (M^2; Figure 2a) is stirred out, resulting in large magnitudes of $\overline{b^{xz}}$ - b_0^{xz}. This results in enhanced potential energy to kinetic energy exchange as compared to the baseline case (Figure 3, green solid line). The decreased stratification condition produces the least variability in cross-front M^2 as a result of a weaker density gradient across the front. As a result, the potential energy to kinetic energy conversion is reduced as compared to the baseline (Figure 3, blue solid line).

For the changing isopycnal slope cases, increased stratification with fixed M^2 results in shallower isopycnal slope (5), and the Eady growth rate ($\propto \frac{f}{\sqrt{Ri}}$) is slower (Figure 4c). The Eady growth rate sets the timescales of mesoscale and submesoscale growth. reducing the amount of energy available for mesoscale instability The inverse is true for the decreased stratification case, where there is an increased Eady growth rate, and mesoscale instabilities evolve faster (Figures 3, blue dotted line). Initial conditions with increased stratification additionally result in a less rapid meridional frontal restratification as compared to the baseline initial conditions. This appears as a less rapid meridional “spreading” of the front. The opposite is true for reduced stratification conditions, where the Eady growth rate is increased (Figure 4e). There is also evidence of enhanced meandering of the front under decreased stratification conditions, resulting in increased shedding of mesoscale eddies carrying frontal properties away from the front and restratifying the upper ocean (not shown).

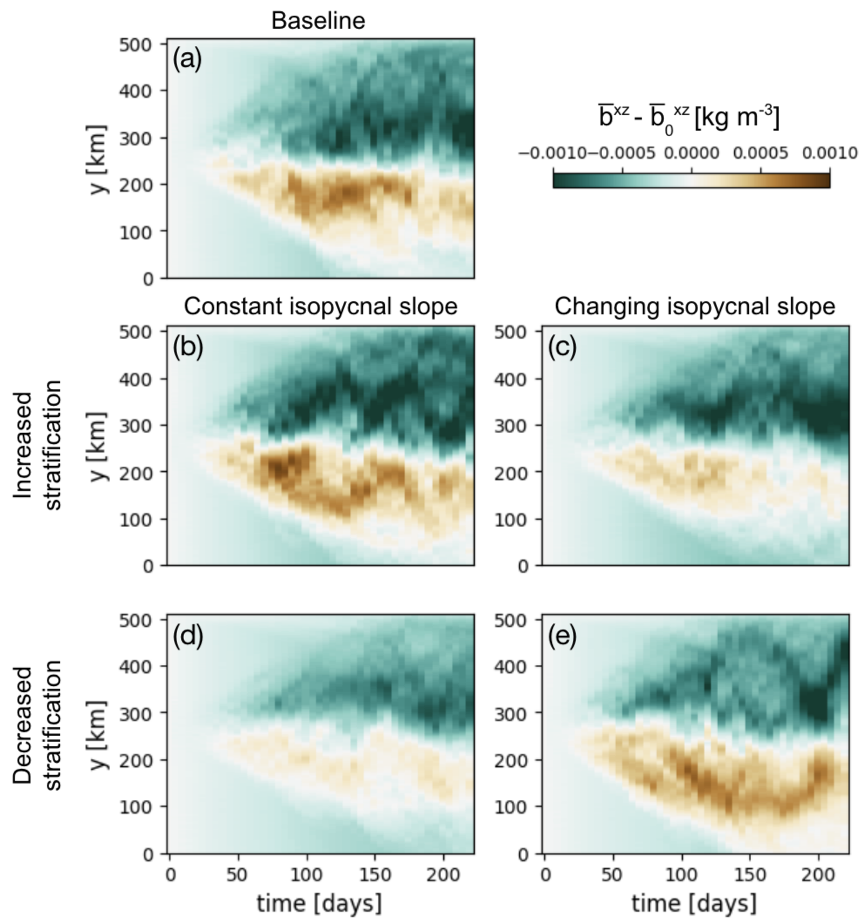

FIG. 4. Time evolution of the front in buoyancy, where $\bar{b}^{xz}$ - b_0^{xz} is the difference between the average buoyancy in the along-front and vertical directions and the initial buoyancy conditions. (a) Baseline conditions, increased stratification conditions for (b) constant slope and (c) changing slope, and decreased stratification conditions for (d) constant slope and (e) changing slope.

Mixed layer depth (MLD) consistently has an inverse relationship with stratification, deepening with decreasing stratification (Figure 5). The range of the response of the MLD to stratification conditions is greater in the cases with a constant isopycnal slope. Under constant isopycnal slope conditions, the MLDs of the increased stratification case are shallower than those for the changing isopycnal slope conditions, and the MLDs of the decreased stratification case are deeper than those for the changing isopycnal slope conditions. The MLD of the decreased stratification cases for both slope conditions are both influenced by a longer tail of deep (> 200 m) MLDs, which are found on the north (light) side of the front.

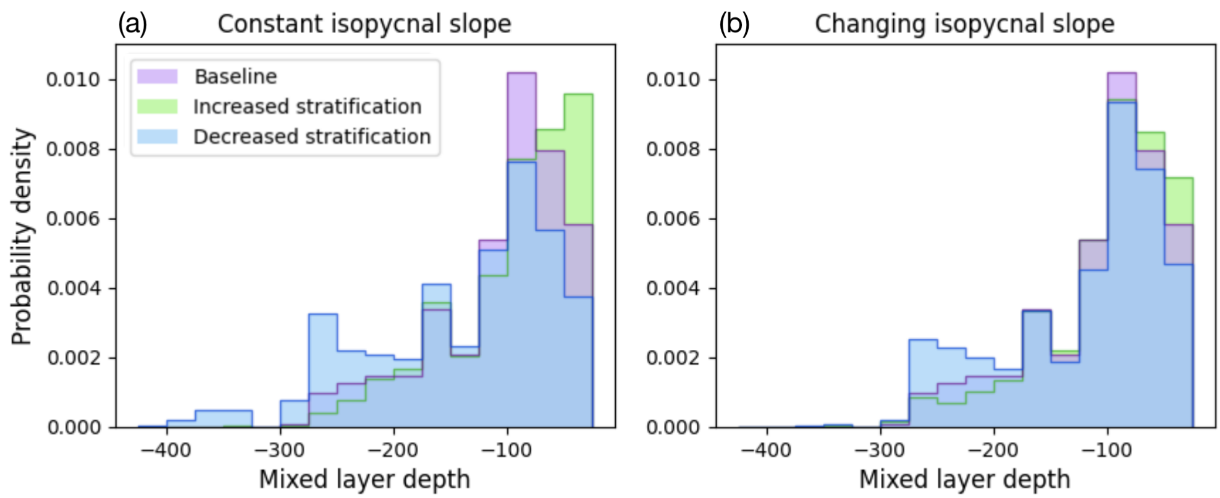

FIG. 5. Mixed layer depth (based on density difference criterion of 0.03 kg m^{-3} from 10 m depth value) for cases with (a) constant isopycnal slope and (b) changing isopycnal slope. MLD is over all gridpoints during tracer experiment (days 199-219).

Subsurface tracer concentration and tracer flux distributions

In the baseline and increased stratification cases, the tracer concentration at 350 m is preferentially located on the north (light) side of the front, while in the decreased stratification case, tracer is located at depth on both sides of the front (Figure 6). For all stratification and slope conditions, features with large (Ro > |.5|) magnitudes are found down to 500 m, consistent with observational evidence of large submesoscale vertical velocities below the base of the mixed layer (Siegelman et al. 2020; Yu et al. 2019). In all stratification cases, high tracer concentration is aligned with anticyclonic features. Specifically, at 350 m 100 days after tracer seeding, 68% of the tracer volume is found within features with $Ro < 0$ at all depths in the baseline case (Figure 7a, Figure S1a). Tracer is disproportionately associated with submesoscale features ($|Ro| > 0.5$), which are only 0.5% of the domain area but account for 4% of the tracer volume, highlighting the importance of these filamentary structures in tracer transport. The relationship between submesoscale dynamics and tracer concentration appears to be shaped by Ro rather than by strain, and the more anticyclonic a feature, the greater the tracer concentration. Lines where $Ro = \sigma$ are pure shear regions, and there are relatively low tracer concentrations associated with these areas. A potential explanation is mean-flow suppression, where the strong horizontal flow at the large-scale front acts as a barrier to along-isopycnal, cross-front eddy-induced transport at the mesoscale and submesoscale (Stamper et al. 2018). This mechanism has been observed in Drake Passage (Naveira Garabato et al. 2011; Dove et al. 2023).

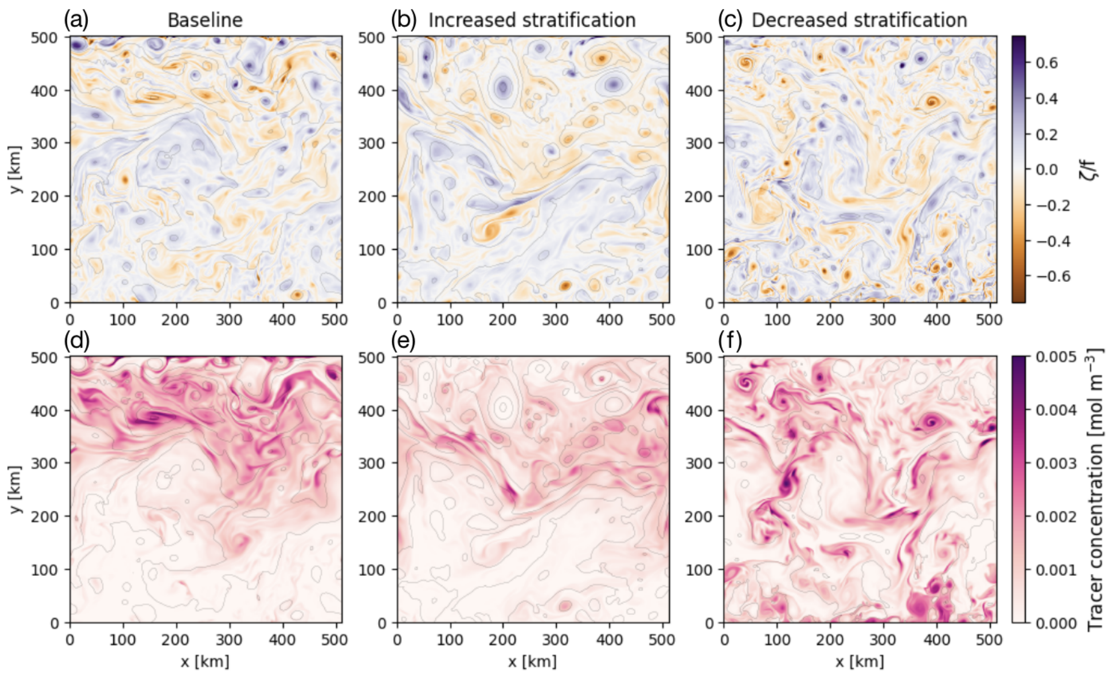

FIG. 6. Comparison of scales of motion across stratification conditions at 350 m at the same timestep (day 219, 49 days after tracer seeding) for simulations under the constant slope conditions. (a)-(c) Rossby number (ζ/f), (d)-(f) tracer concentration [mol m^{-3}]. Gray lines are density contours.

The strongest mean negative (downward) tracer flux is found in anticyclonic features (Figure 7). This negative flux is especially notable in the decreased stratification case. There is less evidence of a preference towards negative flux associated with anticyclonic flow in the increased stratification case. It should be noted that the tracer flux distributions have long tails and are centered near zero, so taking averages reduces the observed strength. Tracer fluxes can in fact reach up to ± 0.2 mol m^{-2} day^{-1}, 20% of the initially seeded tracer, particularly in the decreased stratification case. The vertical velocities associated with these large fluxes are of $O(10)$ m s^{-1}.

Under the condition where the isopycnal slope changes alongside changing N^2, the patterns of tracer concentration and tracer flux look similar across stratification cases (Figure S1). However, the range of Ro in the decreased stratification case is reduced as compared to the constant isopycnal slope case, potentially due to a reduced Eady growth rate (Figures 7c, S1c). There are also fewer points with large, anticyclonic Ro.

In all cases considered, there is evidence of positive tracer flux associated with the edges of the PDFs. There is also evidence of positive tracer flux associated with strong cyclonic features in the constant slope, decreased stratification case. This signature results from later in the simulation, once tracer has been relatively stirred out at depth. At this point, there is potential for the tracer to get upwelled, particularly at high strain regions where frontogenesis can induce vertical motions along sloping isopycnals.

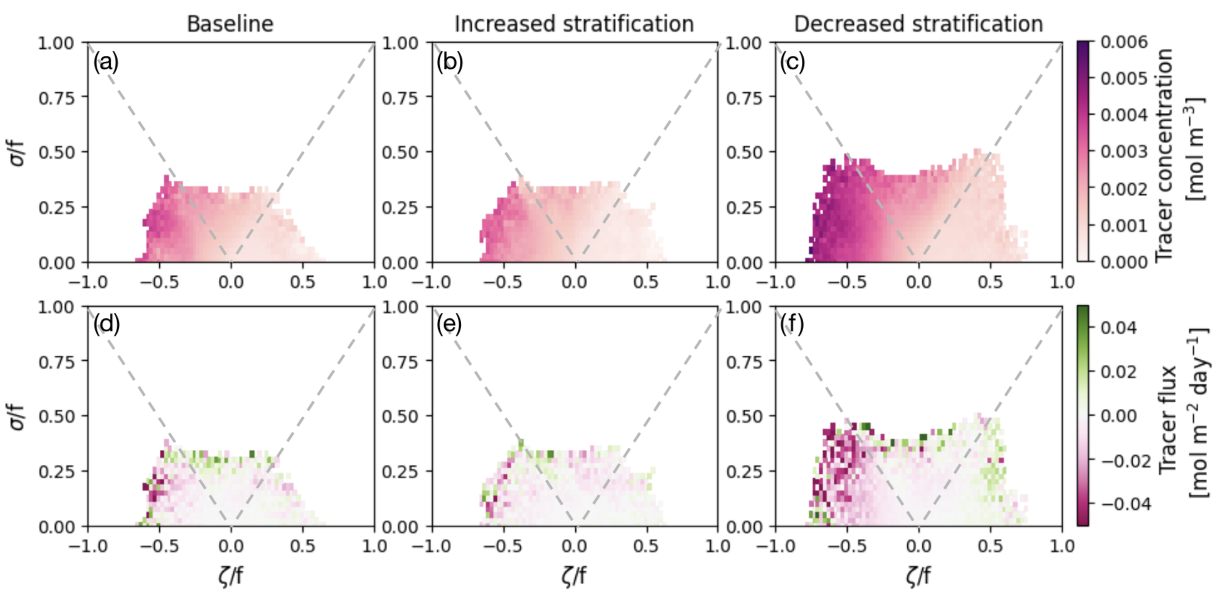

Fig. 7. Joint PDFs of Rossby number (ζ/f) and strain (σ/f) at 350 m with a *constant isopycnal slope* over the tracer experiment (days 199-219). Colored by (a),(c),(e) average tracer concentration [mol m^{-3}] and (b),(d),(f) average tracer flux [mol m^{-2} day^{-1}] per ζ and σ pair. For flux, negative values indicate downwards flux. Grey dashed lines indicate 1:1 ζ/f : σ/f. ζ/f and σ/f pairs with fewer than 10 points are not shown.

When the initial isopycnal slope does not vary, the depth profiles of tracer concentration and tracer flux indicate that stratification impacts the tracer penetration depth (Figure 8). The average concentration of tracer reaching over 500 m is greatest under the decreased stratification conditions, with no tracer reaching below 400 m in increased stratification conditions. More tracer remains within the mixed layer in the increased stratification case as compared to the baseline case. Within the mixed layer in all cases, there is a large, negative (downwards) tracer flux associated with cyclonic features. In anticyclonic features within the mixed layer, there is an associated positive (upwelling) tracer flux, although it is weaker than the positive flux associated with cyclones at the same depth.

The strongest tracer fluxes that cross the average MLD occur at the largest anticyclonic features, the fluxes of which are enhanced between 100 m and 250 m in all stratification cases (Figure 8d-f). The flux associated with anticylonic features is largest in the decreased stratification case, reaching averaged values of up to -0.05 mol m^2 day^{-1} at 400 m.

The depth distribution of the tracer concentration in the changing isopycnal slope conditions varies less than that in the constant slope conditions (Figure S2a-c). Across all stratification regimes, the tracer penetration reaches a maximum of 400 m, with no observable difference in penetration depth. As compared to the constant isopycnal slope case, the decreased stratification case has increased tracer concentration within the mixed layer (Figures 8c and S2c), suggesting less efficient transport of tracer out of the surface layer. As in the constant slope cases, there are strong fluxes within the mixed layer associated with cyclonic features. Although these fluxes are primarily constrained to the mixed layer, there is some penetration of these fluxes below the average MLD, particularly in the decreased stratification case. There are also the same strongest fluxes below the base of the mixed layer associated with the most anticyclonic features.

Mechanism for tracer transport under varying stratification conditions

The anticyclonic features that are associated with strong tracer flux below the base of the mixed layer are highly physically localized to submesoscale anticyclonic eddies that are energized in the mixed layer (Figures 8 and 9). The resulting fluxes can result in "isolated" tracer concentration below the base of the mixed layer (Figure 9h,i). Upon subduction, these boluses can appear disconnected from the surface to the three-dimensional nature of the features, which transport tracer along tilted density surfaces. The observed subduction occurs in regions with strong lateral density gradients, which can be enhanced down to depths greater than 300 m. These subsurface tracer anomalies hold properties akin to the surface (Figure 10a), and have been observed across the global ocean in regions with strong submesoscale flows (Johnson and Omand 2021; Omand et al. 2015; Llort et al. 2018). In the model runs presented here there are larger-scale, weak anticyclonic features (-0.5 < Ro < 0) that are associated with mesoscale eddies, which shape the surface

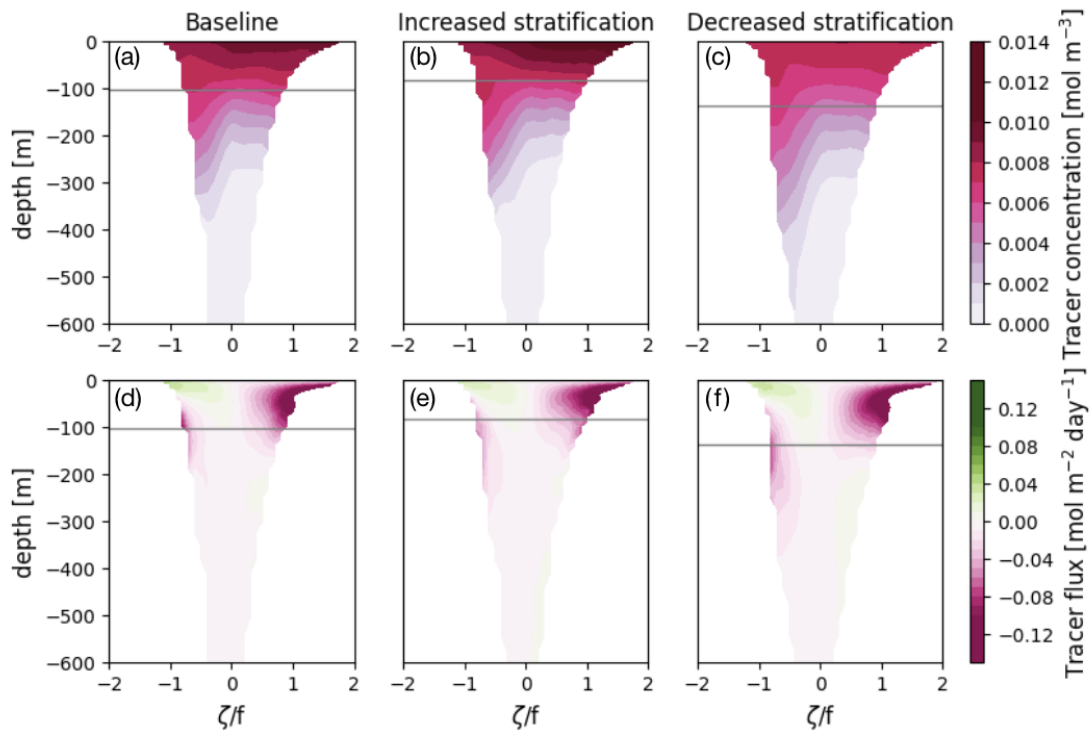

FIG. 8. Tracer concentration and tracer flux as a function of depth and Rossby number with a *constant isopycnal slope* over the tracer experiment (days 199-219). Colored by (a)-(c) average tracer concentration [mol m^{-3}] per Rossby number (ζ/f), weighted by area covered by that Rossby number at that depth. (d)-(f) average tracer flux [mol m^{-2} day^{-1}] per ζ/f. Gray lines represent the average MLD for each stratification case.

distribution of tracer (Figures 9, 10a,b). However, these features, unlike those associated with the strong anticyclonic features, do not necessarily align with subsurface intrusions. Upwelling velocities, which transport low tracer concentration water to the surface, are more diffuse than highly localized downward velocities (Figure 10).

The response of tracer concentration and tracer flux to changing stratification differs between the changing and constant isopycnal slope cases (Figure 11). At given depths, the tracer concentration in constant slope conditions (solid lines) depends on stratification, with decreased stratification resulting in greater tracer concentrations and enhanced negative tracer fluxes. This relationship practically disappears at 500 m depth, pointing towards a mechanism which has its roots in the upper ocean. As pycnocline stratification peaks at 400 m (Figure 1), this means that the majority of tracer transport occurs in the upper pycnocline and out of the mixed layer, but does not cross

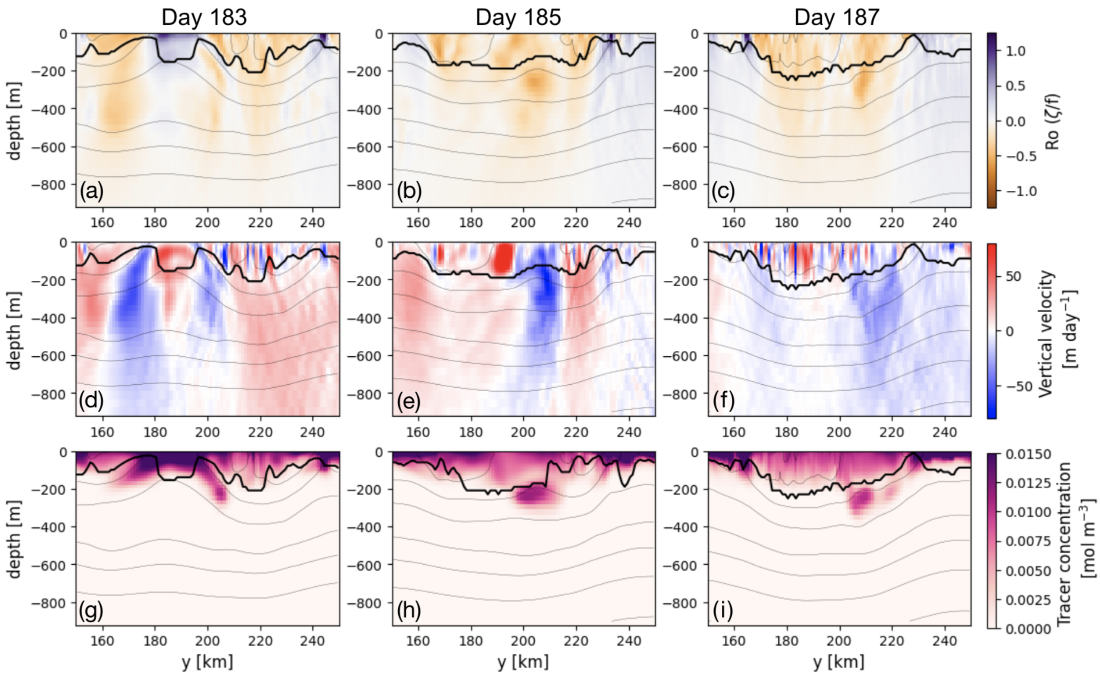

FIG. 9. Tracer subduction and trapping at day 183 (13 days after tracer seeding; column 1), day 185 (15 days after tracer seeding, column 2), and day 187 (17 days after tracer seeding, column 3). (a)-(c) Rossby number (ζ/f), (d)-(f) vertical velocity [m day^{-1}], and (g)-(i) tracer concentration [mol m^{-3}]. Gray lines are density contours. The black line is the MLD.

the pycnocline. This has important implications for the sequestration timescale of these tracers. In increased stratification conditions, tracer flux is not sensitive to further increases in stratification, with the average tracer concentration and tracer fluxes as a function of the initial maximum N^2 plateauing.

Under changing isopycnal slope conditions (Figure 11, dotted lines), there is little to no relationship between changing stratification and tracer concentrations and fluxes. At all depths, tracer concentrations and fluxes remain relatively constant across stratification cases.

The difference between the cases with changing and constant isopycnal slope is explained by investigating the patterns of the strongly anticyclonic features. Examining only features with a *Ro* < -0.5 at 350 m depth, (Figure 12), we find that these strongly anticyclonic features are associated with larger tracer fluxes than the domain average, demonstrating that downward tracer flux is largely performed within these features. This relationship is particularly pronounced in decreased

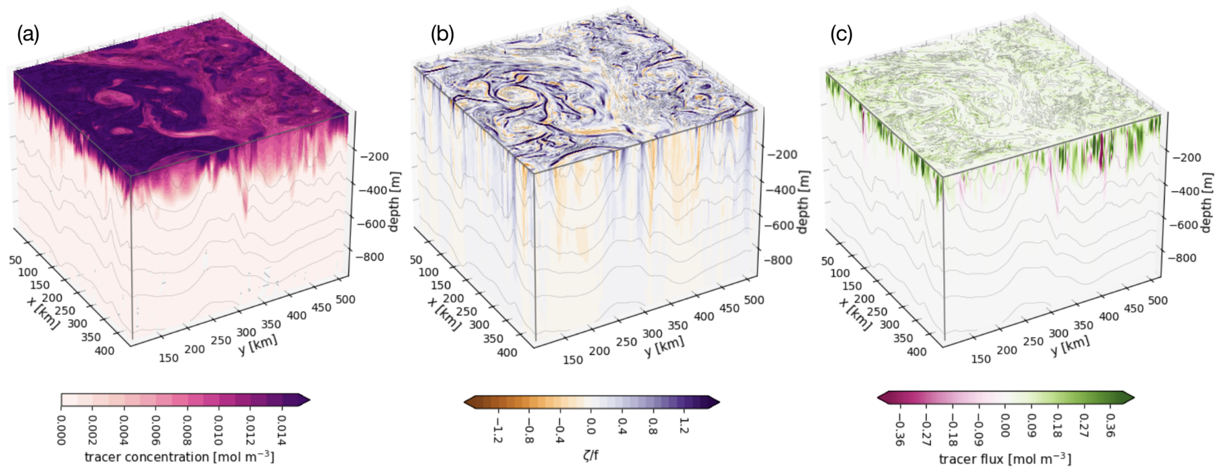

FIG. 10. Subdomain of modeled (a) tracer concentration [mol m^{-3}], (b) Rossby number (ζ/f), and (c) tracer flux [mol m^{-2} day^{-1}] on day 191 (21 days after tracer seeding) of the "baseline" conditions.

stratification conditions, where the weaker the stratification, the greater the magnitude of the associated tracer flux. There is a reduction in downward flux from the baseline to the increased stratification cases. However, as before, the flux reaches a "plateau", although the magnitude of the plateau is still larger than the average across the full domain.

In both conditions where the isopycnal slope is constant and changes, the strongly anticyclonic features are associated with strong downward fluxes (Figure 12a). However, only in conditions with a constant isopycnal slope do the number of points across the domain associated with strongly anticyclonic features increase under decreased stratification conditions (Figure 12b). This is interesting as the available potential energy is actually lower, making the appearance of stronger anticyclones is in that sense counterintuitive. When the isopycnal slope changes, the number of these features does not increase under decreased stratification conditions, so the net tracer flux is significantly reduced as compared to the constant slope case.

The strong anticyclonic features at depth in the reduced stratification (constant initial isopycnal slope) cases are associated with $\mathrm{Ri}_g \sim O(1)$, values that indicate a submesoscale regime. Across the full set of model runs, there are few features where Ri_g is $O(1)$ (Figure S3a,b). There is also evidence that increased stratification conditions in the changing slope conditions result in a shift towards larger Ri_g values, domains that are more shaped by buoyancy stratification rather than shear. It should be noted that the Ri_g distributions in Fig. S3a, b are at 350 m, well out of the

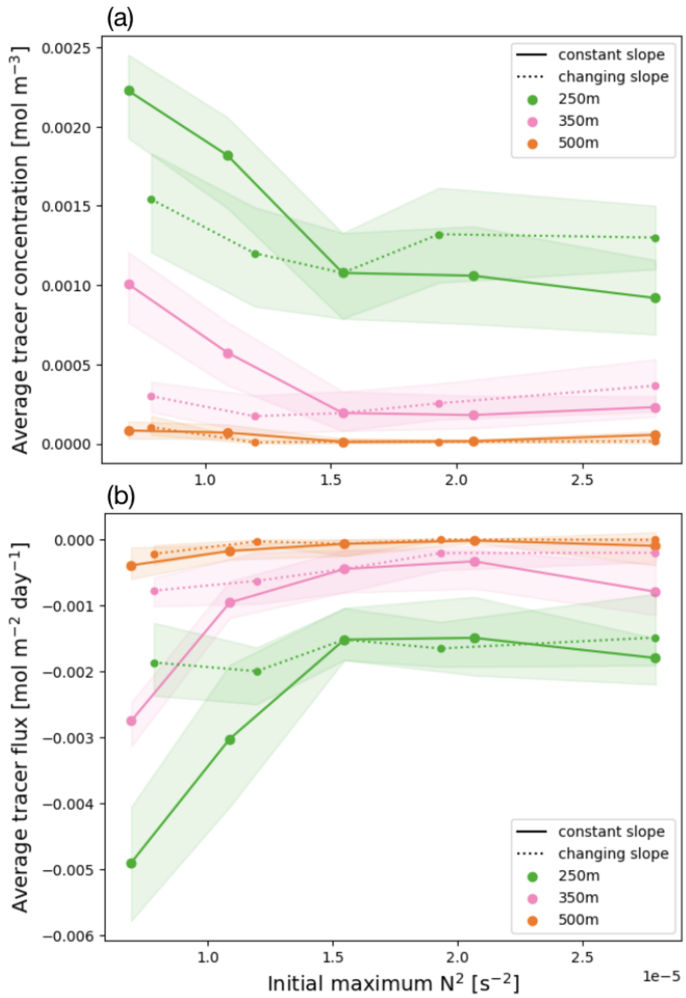

FIG. 11. Averages of tracer concentration and flux at 250 m, 350 m, and 500 m under both constant and isopycnal slope conditions. (a) Spatiotemporal average tracer concentration [mol m^{-3}] and (b) Spatiotemporal average tracer flux [mol m^{-2} day^{-1}]. Shaded regions represent the maximum and minimum spatially averaged values from each timestep during the tracer experiment.

average mixed layer; Ri_g distributions at the surface ocean have significantly longer tails into the $O(1)$ regime.

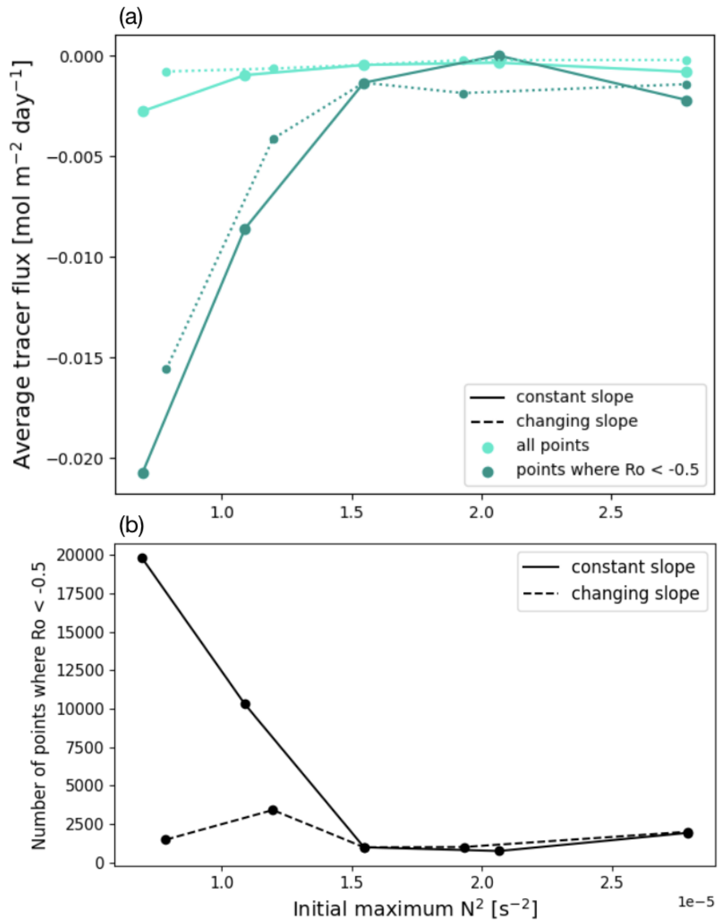

FIG. 12. Flux at 350 m contributed by the full domain and just strongly anticyclonic features. (a) Spatiotemporal average tracer flux per stratification condition performed by the full domain (light blue) and for just features with *Ro* < -0.5 (teal). (b) Number of points with Ro < -0.5 for both the constant and changing isopycnal slope conditions.

4. Discussion

Sensitivity of tracer subduction to changing stratification

The response of vertical tracer subduction to changing stratification is highly dependent on the response of the lateral buoyancy gradient (M^2) to vertical stratification change (N^2). Here, we test two scenarios: (a) where the initial isopycnal slope is held constant by changing M^2 with $M^2 \propto N^2$ and (b) where M^2 is held constant while N^2 and the initial isopycnal slope therefore varies. Although subsurface anticyclonic vortical features (*i.e.* SCVs) are found to be the signature of subduction across these scenarios, tracer fluxes only respond to changing stratification in conditions where the isopycnal slope is held constant. This result highlights the importance of the lateral buoyancy gradient in setting the response of a front to increasing vertical stratification.

We demonstrate that increasing stratification does not necessarily lead to reduced submesoscale tracer transport. Specifically, when the isopycnal slope of an idealized front is initially constant, the magnitude of the tracer flux under increased stratification conditions does not change. Tracer transport reaches a “plateau” under constant slope conditions, suggesting that there may be a point at which increasing stratification of the pycnocline does not have an inverse relationship with downward tracer flux. These results contrast with previous work that has investigated how projected warming scenarios impact submesoscale motions and associated tracer transport by increasing numerical model horizontal viscosity. In these models, submesoscale motions are suppressed (Richards et al. 2021; Wang et al. 2022) and advective carbon export (*i.e.* subduction) out of the surface ocean is largely reduced (Brett et al. 2023). Our idealized model explicitly resolves pycnocline stratification and resolves more submesoscale features due to its 1 km horizontal grid scale (Balwada et al. 2018). Modifying vertical viscosity may not be an appropriate proxy for representing pycnocline stratification change and can result in excessive damping of circulation and mixing processes (Megann and Storkey 2021).

Regarding biogeochemistry, Lévy et al. (2024) recently highlighted the role of submesoscale motions in buffering the negative impacts of climate change on oceanic biogeochemical cycles. They point towards increased stratification decreasing the transport of nutrients to the euphotic layer and the penetration of surface tracers to depth, therefore slowing the physical mechanisms that enable biological productivity. However, our results may demonstrate that if the isopycnal slope will change with increasing stratification, the downward tracer fluxes may already be “at capacity”, and only decreasing stratification would modify tracer transport as a result of increased submesoscale motions, at least under the baseline conditions we tested. The response of all regions to changing stratification is highly dependent on how the lateral buoyancy gradient of ocean density fronts respond to the increasing stratification, which additionally impacts the velocity at the front (Shi et al. 2021). Not investigated in this work, but potentially of additional biogeochemical importance, is the role of stratification in modifying upwelling, which has implications for the entrainment of subsurface-enhanced nutrients into the mixed layer (Uchida et al. 2019; Simoes-Sousa et al. 2022).

Anticyclonic submesoscale coherent vortices are a key subduction pathway

Vertical tracer transport below 350 m preferentially occurs on the north (light) side of the front as there are more anticyclonic features on this side of the front at depth. This is counter to what would typically be expected with a density front, where the dense side of the front "subducts" under the light side of the front and carry surface tracers to depth along isopycnals (Omand et al. 2015; Freilich and Mahadevan 2021). However, due to the deeper mixed layers on the light side of the front, we find the subduction below the base of the mixed layer preferentially occurs here. This aligns with formation of Sub-Antarctic Mode Water (SAMW), which forms to the north of the Polar Front in certain regions of the Southern Ocean (Cerovečki et al. 2013; Naveira Garabato et al. 2009) and points to the potential contribution of submesoscale motions to SAMW ventilation.

There are many physical processes at the submesoscale that can contribute to downward tracer fluxes out of the ocean mixed layer that are not well-resolved in these simulations (*e.g.* Ekman buoyancy flux and symmetric instability). Full reviews are available in Thomas et al. (2013) and Taylor and Thompson (2023), parameterization in Bachman et al. (2017), and enhanced turbulent entrainment guided by submesoscale structures described in Smith et al. (2016). In our simulations, within the mixed layer, tracer is preferentially trapped in cyclonic eddies, primarily at the scale of the mesoscale. However, at depth (*e.g.* 350m, Figures 6 and 7), tracer is preferentially found within anticyclonic features at large Rossby number, so based on the dynamical definition these are submesoscale features. At the surface, cyclones are predominantly associated with $w<0$ and anticyclones with $w>0$. However, this trend reverses starting around 50 m, where anticyclones can be associated with w<0, and the downward flux by anticyclonic features reflects this shift (Figures 8 and S2). Cyclonic features preferentially gather tracer at the surface and at intense submesoscale fronts this tracer is subducted along steeply tilted isopycnals (Figure 9). During this process, tracer moves from the dense side of the submesoscale front to the light side (Pham et al. 2024), where it gets trapped. Because the isopycnal layer in which the subducted parcel is trapped is thinner than the depth of the mixed layer from which it was subducted, the parcel "spins down" and becomes anticyclonic (Spall 1995). The resulting anticyclonic submesoscale coherent vortices (SCVs; McWilliams (1985); Dewar and Meng (1995)) are characterised by Ro $O(1)$ and are retained in the interior until being stirred out by the mesoscale strain field that acts to homogenize the tracer field at depth after subduction. The frontal generation mechanism contrasts with previous work which has emphasized the role of flow-topography interactions (Vic et al. 2018; Gula et al. 2019; Bosse et al. 2015), deep convection (Bosse et al. 2016; Lilly and Rhines 2002), and eddy-wind interactions (Thomas 2008; McGillicuddy 2015) in the generation of SCVs, although the latter two may play some role in this case. The observed vorticity decrease upon subduction is slightly underestimated by quasi-geostrophic vorticity scaling, suggesting an important role for ageostrophic dynamics in the generation of and tracer transport by SCVs.

The frequency of SCVs explains the relative sensitivity of the constant isopycnal case to stratification. SCVs are preferentially formed in the modeled decreased stratification conditions as compared to the baseline conditions (Figure 6). Deeper mixed layers associated with the decreased stratification conditions provide deeper subduction of the surface tracer. Although there is not necessarily more submesoscale structure in decreased stratification conditions (Figures 3 and 8), surface-enhanced submesoscale vertical velocities can penetrate more deeply with low stratification. This contrasts with the varying isopycnal slope case where reduced stratification does not facilitate the formation of SCVs.

The result that coherent anticyclones transport tracers from the mixed layer to the interior appears to be consistent with previous observations of tracer transport out of deep mixed layers in subpolar regions (Omand et al. 2015). At the same time, our results are not inconsistent with recent results that cyclonic features at fronts are vital for subduction across the mixed layer base, and play a leading order role in transporting phytoplankton out of the photic zone (Freilich et al. 2024; Freilich and Mahadevan 2021). Features with $Ro > |0.5|$ below of the mixed layer are rarely described in the observational literature, partly due to the challenge of measuring *Ro in situ* and partly due to the highly localized nature of these features (Buckingham et al. 2016). However, recent observations of density gradients and subsurface velocity provide evidence of submesoscale gradients at depth (Siegelman et al. 2020; Yu et al. 2019). Our results complement these findings, highlighting the biogeochemical component of this exchange. However, previous research has identified low stratification features in the ocean interior and attributed these to subduction from the mixed layer by mixed layer eddies (Omand et al. 2015; Llort et al. 2018; Johnson and Omand 2021). These are consistent with being generated by the mechanisms discussed in this manuscript and our results demonstrate their sensitivity to pycnocline stratification and the mean flow in the Southern Ocean, factors which are not included in previous scaling estimates of the biogeochemical flux by these features. SCVs do not penetrate the strongest pycnocline (peak at 500 m) in this experiment. The surface cooling of our model is meant to resemble springtime; wintertime surface forcing may provide more insight into the potential for sub-pycnocline tracer transport.

Increased attention should be paid to subsurface anticyclonic features in future field studies focused on constraining and quantifying carbon export, with explicit focus on the sign of the vorticity of the submesoscale eddy. SCVs are particularly of interest for tracer budgets due to the capacity of these features to transport tracers away from the location of subduction and biogeochemcial property anomalies can be a characteristic of SCVs (McWilliams 1985). SCVs and Deep Coherent Vortices (DCVs) of known origin, such as anticyclonic Meddies formed from the Mediterranean Undercurrent as it enters the Atlantic, tend to have a preference for cyclonic or anticyclonic rotation. These features may play a leading-order role in tracer sequestration below the base of the mixed layer, particularly in highly energetic regions of the open ocean such as the Gulf Stream (Gula et al. 2019) and Southern Ocean (Lazaneo et al. 2022). SCVs and DCVs do not necessarily have a surface expression (Assassi et al. 2016), highlighting the continued need for subsurface observations to estimate tracer fluxes by these processes that work both vertically and laterally. It is additionally difficult to detect them using single profiles, such as from Argo floats, because the relevant background stratification may be hard to estimate (McCaffrey et al. 2015).

The current parameterization primarily employed in climate models to restratify the ocean mixed layer represents the physics of mixed layer instability (MLI; Fox-Kemper et al. (2008)). MLI will occur in any region where lateral buoyancy gradients provide a source of potential energy; however, the effectiveness of MLI in transporting tracers below the base of the mixed layer is highly dependent on the background conditions. In particular, submesoscale motions are typically strongest in wintertime (Callies et al. 2015; Su et al. 2018) when mixed layers are deep. The stratification of the pycnocline can be expected to also play a role in the effectiveness of MLI for tracer subduction, with stronger stratification resulting in a barrier to penetration; however, these motions can still be important for transporting tracer to the base of the mixed layer, at which point they can be stirred out by the mesoscale flow (Freilich et al. 2024). In the context of biology, the base of the mixed layer may be out of the photic zone, halting further biological production. The Fox-Kemper et al. (2008) parameterization uses a streamfunction parameterization for vertical velocities in the mixed layer, which assumes vertical velocities approach zero at the base of the mixed layer. Therefore, MLI as currently parameterized in global climate models cannot result in tracer fluxes across the base of the mixed layer. This limitation may not present a problem when there is strong stratification at the bottom limit of the streamfunction (*e.g.* the mixed layer base), as demonstrated in our results. However, in conditions where background stratification is low, capping the overturning streamfunction to only the mixed layer may result in a inaccurate representation of the true tracer fluxes.

Implications for future tracer subduction and applications to the Antarctic Circumpolar Current

The impact of increasing pycnocline stratification on tracer subduction at fronts is highly dependent on the response of the frontal lateral buoyancy gradient. When the lateral buoyancy gradient "adjusts" to maintain a constant isopycnal slope, the impacts of increased stratification on tracer subduction are minimal in the regime studied here, but the impacts of decreased stratification are significant for tracer transport. The relationship between pycnocline stratification and tracer flux is relatively linear when considering conditions with less stratification than the baseline case. With decreased stratification, there is evidence of enhanced anticyclonic submesoscale motions below the MLD, which readily transport tracers from the surface into the interior domain. However, there appears to be a limit on the relationship between tracer flux and increasing stratification with a constant isopycnal slope; increasing stratification beyond 1.5 e^{-5} s^{-2} in the context of our experiment has minimal impacts on the tracer transport, observed by the "plateau" of tracer concentrations and fluxes. Regardless of pycnocline stratification, when the isopycnal slope varies as a result of holding the surface lateral buoyancy gradient constant, tracer fluxes are constant.

Given these modeled conditions were chosen to mimic the Antarctic Polar Front, this result has implications for future tracer uptake at the Polar Front, which is a major location for surface tracer subduction to depth by submesoscale motions (Dove et al. 2021; Balwada et al. 2024; Llort et al. 2018). Current observations across the Southern Ocean (Sallée et al. 2021) suggest an increasing pycnocline stratification at a rate of $8.1 \pm 4.1\%$ dec^{-1}. With this rate of increase, it would take 30 ± 20 years to reach the modeled increased stratification (1.9 $e^{-5}s^{-2}$ under changing slope conditions). Our idealized model suggests that increased stratification may not change tracer transport at the submesoscale, no matter how the slope of the ACC responds. Care should be taken when extrapolating these results, however, as salinity is traditionally considered the primary control on density south of the Polar Front and our model only uses temperature as an active tracer. In addition, rate of stratification increase may change as a result of changing buoyancy forces (*e.g.* changing location and magnitude of sea ice melt; Hobbs et al. (2016)). Our model is semi-idealized and may not accurately capture the complexities of the ACC, where some regions have a reduced "baseline" stratification. Moreover, our model only includes the upper ocean front and does not represent the overturning circulation in the Southern Ocean.

Changes to the isopycnal slope across the ACC have been minimal in a basin-wide context (Böning et al. 2008), suggesting that our scenario that holds the isopycnal slope constant is the relevant case for observational comparisons. However, the response to increasing stratification may be more local. Specifically, standing meanders of the ACC, resulting from flow-topography interactions, are associated with enhanced eddy kinetic energy (Sokolov and Rintoul 2007; Klocker 2018; Yung et al. 2022). These regions have been demonstrated to be areas where not only are mesoscale eddies preferentially generated due to strongly sloped isopycnals (Thompson and Naveira Garabato 2014; Chapman et al. 2015), but also are areas where there is enhanced tracer variance on isopycnal surfaces at the submesoscale (Dove et al. 2021; Balwada et al. 2024). High eddy kinetic energy areas are also known to be regions where both tracer entertainment (Tamsitt et al. 2017; Brady et al. 2021) and isolation from the surface mixed layer (Dove et al. 2022) occurs. Our idealized model results suggest that these highly dynamical regions may be strongly impacted by increasing stratification across the Southern Ocean, especially because the average pycnocline stratification is reduced in these regions (Sallée et al. 2021).

5. Conclusion

Using a suite of idealized numerical simulations, we illustrate that decreased stratification across the global ocean may increase the capacity for submesoscale motions to transport tracers from the surface mixed layer into the interior ocean. This transport occurs disproportionately within strongly anticyclonic submesoscale eddies, which regularly transports tracer from the mixed layer to >400 m. The impact of the change in stratification is strongly dependent on whether oceanic fronts have a corresponding response of their horizontal density gradient, with fronts that have a changing isopycnal slope not demonstrating variability in fluxes by these submesoscale motions. Under increased stratification conditions, as are underway with a warming ocean, the tracer transport reaches a "plateau", suggesting that there may be a point at which increasing stratification of the pycnocline does not have an inverse relationship with downward tracer flux. The initial conditions tested here mimic those of a relatively quiescent region of the ACC; the results suggest that regardless of how the isopycnal slope of the ACC responds to increasing stratification, submesoscale tracer transport may be saturated and not change in the coming century.

Acknowledgments. LAD was funded by a NOAA Climate & Global Change Postdoctoral Fellowship and thanks the staff at the Cooperative Programs for the Advancement of Earth System Science for their adaptability and assistance. MAF was supported by NASA grant 80NSSC24K0410. BFK was supported by NSF 2149041. The authors thank Élise Beaudin for useful discussions during the production of this research.

Data availability statement. Float data from Snapshot 2023-08-28 (`https://doi.org/10.6075/J0542NS9`) were collected and made freely available by the Southern Ocean Carbon and Climate Observations and Modeling (SOCCOM) Project funded by the National Science Foundation, Division of Polar Programs (NSF PLR-1425989 with extension NSF OPP-1936222) supplemented by NASA and by the International Argo Program and the NOAA programs that contribute to it. The Argo Program is part of the Global Ocean Observing System (`https://doi.org/10.17882/42182`).

The model simulation files are available and documented at `doi.org/10.5281/zenodo.13937157`.

References

Assassi, C., and Coauthors, 2016: An Index to Distinguish Surface- and Subsurface-Intensified Vortices from Surface Observations. https://doi.org/10.1175/JPO-D-15-0122.1.

Bachman, S. D., B. Fox-Kemper, J. R. Taylor, and L. N. Thomas, 2017: Parameterization of Frontal Symmetric Instabilities. I: Theory for Resolved Fronts. *Ocean Modelling*, **109**, 72–95, https://doi.org/10.1016/j.ocemod.2016.12.003.

Balwada, D., A. R. Gray, L. A. Dove, and A. F. Thompson, 2024: Tracer Stirring and Variability in the Antarctic Circumpolar Current Near the Southwest Indian Ridge. *Journal of Geophysical Research: Oceans*, **129 (1)**, e2023JC019 811, https://doi.org/10.1029/2023JC019811.

Balwada, D., K. S. Smith, and R. P. Abernathey, 2018: Submesoscale Vertical Velocities Enhance Tracer Subduction in an Idealized Antarctic Circumpolar Current. *Geophysical Research Letters*, **45 (18)**, 9790–9802, https://doi.org/10.1029/2018GL079244.

Behrenfeld, M. J., and Coauthors, 2006: Climate-driven trends in contemporary ocean productivity. *Nature*, **444 (7120)**, 752–755, https://doi.org/10.1038/nature05317.

Bosse, A., P. Testor, L. Mortier, L. Prieur, V. Taillandier, F. d'Ortenzio, and L. Coppola, 2015: Spreading of Levantine Intermediate Waters by submesoscale coherent vortices in the northwestern Mediterranean Sea as observed with gliders. *Journal of Geophysical Research: Oceans*, **120 (3)**, 1599–1622, https://doi.org/10.1002/2014JC010263.

Bosse, A., and Coauthors, 2016: Scales and dynamics of Submesoscale Coherent Vortices formed by deep convection in the northwestern Mediterranean Sea. *Journal of Geophysical Research: Oceans*, **121 (10)**, 7716–7742, https://doi.org/10.1002/2016JC012144.

Bourgeois, T., N. Goris, J. Schwinger, and J. F. Tjiputra, 2022: Stratification constrains future heat and carbon uptake in the Southern Ocean between 30°S and 55°S. *Nature Communications*, **13 (1)**, 340, https://doi.org/10.1038/s41467-022-27979-5.

Boyd, P. W., H. Claustre, M. Lévy, D. A. Siegel, and T. Weber, 2019: Multi-faceted particle pumps drive carbon sequestration in the ocean. *Nature*, **568 (7752)**, 327, https://doi.org/10.1038/s41586-019-1098-2.

Brady, R. X., M. E. Maltrud, P. J. Wolfram, H. F. Drake, and N. S. Lovenduski, 2021: The Influence of Ocean Topography on the Upwelling of Carbon in the Southern Ocean. *Geophysical Research Letters*, **48 (19)**, e2021GL095 088, https://doi.org/10.1029/2021GL095088.

Brannigan, L., 2016: Intense submesoscale upwelling in anticyclonic eddies. *Geophysical Research Letters*, **43 (7)**, 3360–3369, https://doi.org/10.1002/2016GL067926.

Brett, G. J., D. B. Whitt, M. C. Long, F. O. Bryan, K. Feloy, and K. J. Richards, 2023: Submesoscale Effects on Changes to Export Production Under Global Warming. *Global Biogeochemical Cycles*, **37 (3)**, e2022GB007 619, https://doi.org/10.1029/2022GB007619.

Buckingham, C. E., and Coauthors, 2016: Seasonality of submesoscale flows in the ocean surface boundary layer. *Geophysical Research Letters*, **43 (5)**, 2118–2126, https://doi.org/10.1002/2016GL068009.

Böning, C. W., A. Dispert, M. Visbeck, S. R. Rintoul, and F. U. Schwarzkopf, 2008: The response of the Antarctic Circumpolar Current to recent climate change. *Nature Geoscience*, **1 (12)**, 864–869, https://doi.org/10.1038/ngeo362.

Callies, J., R. Ferrari, J. M. Klymak, and J. Gula, 2015: Seasonality in submesoscale turbulence. *Nature Communications*, **6 (1)**, 6862, https://doi.org/10.1038/ncomms7862.

Cao, H., and Coauthors, 2024: Isopycnal Submesoscale Stirring Crucially Sustaining Subsurface Chlorophyll Maximum in Ocean Cyclonic Eddies. *Geophysical Research Letters*, **51 (4)**, e2023GL105 793, https://doi.org/10.1029/2023GL105793.

Cerovečki, I., L. D. Talley, M. R. Mazloff, and G. Maze, 2013: Subantarctic Mode Water Formation, Destruction, and Export in the Eddy-Permitting Southern Ocean State Estimate. *Journal of Physical Oceanography*, **43 (7)**, 1485–1511, https://doi.org/10.1175/JPO-D-12-0121.1.

Chapman, C. C., A. M. Hogg, A. E. Kiss, and S. R. Rintoul, 2015: The Dynamics of Southern Ocean Storm Tracks. *Journal of Physical Oceanography*, **45 (3)**, 884–903, https://doi.org/10.1175/JPO-D-14-0075.1.

Constantinou, N. C., and A. M. Hogg, 2019: Eddy Saturation of the Southern Ocean: A Baroclinic Versus Barotropic Perspective. *Geophysical Research Letters*, **46 (21)**, 12 202–12 212, https://doi.org/https://doi.org/10.1029/2019GL084117.

Dewar, W. K., and H. Meng, 1995: The Propagation of Submesoscale Coherent Vortices.

Dove, L. A., D. Balwada, A. F. Thompson, and A. R. Gray, 2022: Enhanced Ventilation in Energetic Regions of the Antarctic Circumpolar Current. *Geophysical Research Letters*, **49 (13)**, e2021GL097 574, https://doi.org/10.1029/2021GL097574.

Dove, L. A., A. F. Thompson, D. Balwada, and A. R. Gray, 2021: Observational Evidence of Ventilation Hotspots in the Southern Ocean. *Journal of Geophysical Research: Oceans*, **126 (7)**, e2021JC017 178, https://doi.org/10.1029/2021JC017178.

Dove, L. A., G. A. Viglione, A. F. Thompson, M. M. Flexas, T. R. Cason, and J. Sprintall, 2023: Controls on Wintertime Ventilation in Southern Drake Passage. *Geophysical Research Letters*, **50 (5)**, e2022GL102 550, https://doi.org/10.1029/2022GL102550.

Downes, S. M., A. S. Budnick, J. L. Sarmiento, and R. Farneti, 2011: Impacts of wind stress on the Antarctic Circumpolar Current fronts and associated subduction. *Geophysical Research Letters*, **38 (11)**, https://doi.org/10.1029/2011GL047668.

Fedorov, A. V., R. C. Pacanowski, S. G. Philander, and G. Boccaletti, 2004: The Effect of Salinity on the Wind-Driven Circulation and the Thermal Structure of the Upper Ocean.

Fox-Kemper, B., R. Ferrari, and R. Hallberg, 2008: Parameterization of Mixed Layer Eddies. Part I: Theory and Diagnosis. *Journal of Physical Oceanography*, **38 (6)**, 1145–1165, https://doi.org/10.1175/2007JPO3792.1.

Fox-Kemper, B., and D. Menemenlis, 2008: Can Large Eddy Simulation Techniques Improve Mesoscale Rich Ocean Models? *Ocean Modeling in an Eddying Regime*, American Geophysical Union (AGU), 319–337, https://doi.org/10.1029/177GM19, URL https://onlinelibrary.wiley.com/doi/abs/10.1029/177GM19, _eprint: https://agupubs.onlinelibrary.wiley.com/doi/pdf/10.1029/177GM19.

Freilich, M. A., and A. Mahadevan, 2021: Coherent Pathways for Subduction From the Surface Mixed Layer at Ocean Fronts. *Journal of Geophysical Research: Oceans*, **126 (5)**, e2020JC017 042, https://doi.org/10.1029/2020JC017042.

Freilich, M. A., and Coauthors, 2024: 3D intrusions transport active surface microbial assemblages to the dark ocean. *Proceedings of the National Academy of Sciences*, **121 (19)**, e2319937 121, https://doi.org/10.1073/pnas.2319937121.

Gula, J., T. M. Blacic, and R. E. Todd, 2019: Submesoscale Coherent Vortices in the Gulf Stream. *Geophysical Research Letters*, **46 (5)**, 2704–2714, https://doi.org/10.1029/2019GL081919.

Hobbs, W. R., R. Massom, S. Stammerjohn, P. Reid, G. Williams, and W. Meier, 2016: A review of recent changes in Southern Ocean sea ice, their drivers and forcings. *Global and Planetary Change*, **143**, 228–250, https://doi.org/10.1016/j.gloplacha.2016.06.008.

Hogg, A. M., M. P. Meredith, D. P. Chambers, E. P. Abrahamsen, C. W. Hughes, and A. K. Morrison, 2015: Recent trends in the Southern Ocean eddy field. *Journal of Geophysical Research: Oceans*, **120 (1)**, 257–267, https://doi.org/https://doi.org/10.1002/2014JC010470.

Hordoir, R., and Coauthors, 2022: Changes in Arctic Stratification and Mixed Layer Depth Cycle: A Modeling Analysis. *Journal of Geophysical Research: Oceans*, **127 (1)**, e2021JC017 270, https://doi.org/10.1029/2021JC017270.

Johnson, A. R., and M. M. Omand, 2021: Evolution of a Subducted Carbon-Rich Filament on the Edge of the North Atlantic Gyre. *Journal of Geophysical Research: Oceans*, **126 (2)**, e2020JC016 685, https://doi.org/10.1029/2020JC016685.

Klein, P., and G. Lapeyre, 2009: The Oceanic Vertical Pump Induced by Mesoscale and Submesoscale Turbulence. *Annual Review of Marine Science*, **1 (1)**, 351–375, https://doi.org/10.1146/annurev.marine.010908.163704.

Klocker, A., 2018: Opening the window to the Southern Ocean: The role of jet dynamics. *Science Advances*, **4 (10)**, eaao4719, https://doi.org/10.1126/sciadv.aao4719.

Lazaneo, C. Z., P. H. R. Calil, A. Tandon, and I. C. A. da Silveira, 2022: Submesoscale Coherent Vortices in the South Atlantic Ocean: A Pathway for Energy Dissipation. *Journal of Geophysical Research: Oceans*, **127 (2)**, e2020JC017 099, https://doi.org/10.1029/2020JC017099.

Li, G., L. Cheng, J. Zhu, K. E. Trenberth, M. E. Mann, and J. P. Abraham, 2020: Increasing ocean stratification over the past half-century. *Nature Climate Change*, **10 (12)**, 1116–1123, https://doi.org/10.1038/s41558-020-00918-2.

Lilly, J. M., and P. B. Rhines, 2002: Coherent Eddies in the Labrador Sea Observed from a Mooring.

Llort, J., C. Langlais, R. Matear, S. Moreau, A. Lenton, and P. G. Strutton, 2018: Evaluating Southern Ocean Carbon Eddy-Pump From Biogeochemical-Argo Floats. *Journal of Geophysical Research: Oceans*, **123 (2)**, 971–984, https://doi.org/10.1002/2017JC012861.

Luo, Y., and J. Callies, 2023: Vertical Exchange Induced by Mixed Layer Instabilities. https://doi.org/10.1175/JPO-D-23-0059.1.

Luyten, J. R., J. Pedlosky, and H. Stommel, 1983: The Ventilated Thermocline.

Lévy, M., D. Couespel, C. Haëck, M. G. Keerthi, I. Mangolte, and C. J. Prend, 2024: The Impact of Fine-Scale Currents on Biogeochemical Cycles in a Changing Ocean. *Annual Review of Marine Science*, **16 (Volume 16, 2024)**, 191–215, https://doi.org/10.1146/annurev-marine-020723-020531.

Lévy, M., P. J. S. Franks, and K. S. Smith, 2018: The role of submesoscale currents in structuring marine ecosystems. *Nature Communications*, **9 (1)**, 4758, https://doi.org/10.1038/s41467-018-07059-3.

Mahadevan, A., 2016: The Impact of Submesoscale Physics on Primary Productivity of Plankton. *Annual Review of Marine Science*, **8 (1)**, 161–184, https://doi.org/10.1146/annurev-marine-010814-015912.

Marshall, J., A. Adcroft, C. Hill, L. Perelman, and C. Heisey, 1997: A finite-volume, incompressible Navier Stokes model for studies of the ocean on parallel computers. *Journal of Geophysical Research: Oceans*, **102 (C3)**, 5753–5766, https://doi.org/10.1029/96JC02775.

Martínez-Moreno, J., A. M. Hogg, M. H. England, N. C. Constantinou, A. E. Kiss, and A. K. Morrison, 2021: Global changes in oceanic mesoscale currents over the satellite altimetry record. *Nature Climate Change*, 1–7, https://doi.org/10.1038/s41558-021-01006-9.

McCaffrey, K., B. Fox-Kemper, and G. Forget, 2015: Estimates of Ocean Macroturbulence: Structure Function and Spectral Slope from Argo Profiling Floats. https://doi.org/10.1175/JPO-D-14-0023.1.

McGillicuddy, D. J., 2015: Formation of Intrathermocline Lenses by Eddy–Wind Interaction. https://doi.org/10.1175/JPO-D-14-0221.1.

McGillicuddy, D. J., 2016: Mechanisms of Physical-Biological-Biogeochemical Interaction at the Oceanic Mesoscale. *Annual Review of Marine Science*, **8 (1)**, 125–159, https://doi.org/10.1146/annurev-marine-010814-015606.

McWilliams, J. C., 1985: Submesoscale, coherent vortices in the ocean. *Reviews of Geophysics*, **23 (2)**, 165–182, https://doi.org/10.1029/RG023i002p00165.

McWilliams, J. C., 2019: A survey of submesoscale currents. *Geoscience Letters*, **6 (1)**, 3, https://doi.org/10.1186/s40562-019-0133-3.

Megann, A., and D. Storkey, 2021: Exploring Viscosity Space in an Eddy-Permitting Global Ocean Model: Is Viscosity a Useful Control for Numerical Mixing? *Journal of Advances in Modeling Earth Systems*, **13 (5)**, e2020MS002 263, https://doi.org/10.1029/2020MS002263.

Meredith, M. P., A. C. N. Garabato, A. M. Hogg, and R. Farneti, 2012: Sensitivity of the Overturning Circulation in the Southern Ocean to Decadal Changes in Wind Forcing. https://doi.org/10.1175/2011JCLI4204.1.

Montégut, C. d. B., G. Madec, A. S. Fischer, A. Lazar, and D. Iudicone, 2004: Mixed layer depth over the global ocean: An examination of profile data and a profile-based climatology. *Journal of Geophysical Research: Oceans*, **109 (C12)**, https://doi.org/10.1029/2004JC002378.

Morrison, A. K., and A. M. Hogg, 2013: On the Relationship between Southern Ocean Overturning and ACC Transport. *Journal of Physical Oceanography*, **43 (1)**, 140–148, https://doi.org/10.1175/JPO-D-12-057.1.

Munday, D. R., H. L. Johnson, and D. P. Marshall, 2013: Eddy Saturation of Equilibrated Circumpolar Currents. *Journal of Physical Oceanography*, **43 (3)**, 507–532, https://doi.org/10.1175/JPO-D-12-095.1.

Naveira Garabato, A. C., R. Ferrari, and K. L. Polzin, 2011: Eddy stirring in the Southern Ocean. *Journal of Geophysical Research: Oceans*, **116 (C9)**, https://doi.org/10.1029/2010JC006818.

Naveira Garabato, A. C., L. Jullion, D. P. Stevens, K. J. Heywood, and B. A. King, 2009: Variability of Subantarctic Mode Water and Antarctic Intermediate Water in the Drake Passage during the Late-Twentieth and Early-Twenty-First Centuries. *Journal of Climate*, **22 (13)**, 3661–3688, https://doi.org/10.1175/2009JCLI2621.1.

Newsom, E., L. Zanna, and J. Gregory, 2023: Background Pycnocline Depth Constrains Future Ocean Heat Uptake Efficiency. *Geophysical Research Letters*, **50 (22)**, e2023GL105 673, https://doi.org/10.1029/2023GL105673.

Omand, M. M., E. A. D'Asaro, C. M. Lee, M. J. Perry, N. Briggs, I. Cetinić, and A. Mahadevan, 2015: Eddy-driven subduction exports particulate organic carbon from the spring bloom. *Science*, **348 (6231)**, 222–225, https://doi.org/10.1126/science.1260062.

Pham, H. T., V. Verma, S. Sarkar, A. Y. Shcherbina, and E. A. D'Asaro, 2024: Rapid Downwelling of Tracer Particles Across the Boundary Layer and Into the Pycnocline at Submesoscale Ocean Fronts. *Geophysical Research Letters*, **51 (17)**, e2024GL109 674, https://doi.org/10.1029/2024GL109674.

Richards, K. J., D. B. Whitt, G. Brett, F. O. Bryan, K. Feloy, and M. C. Long, 2021: The Impact of Climate Change on Ocean Submesoscale Activity. *Journal of Geophysical Research: Oceans*, **126 (5)**, e2020JC016 750, https://doi.org/10.1029/2020JC016750.

Roch, M., P. Brandt, and S. Schmidtko, 2023: Recent large-scale mixed layer and vertical stratification maxima changes. *Frontiers in Marine Science*, **10**, https://doi.org/10.3389/fmars.2023.1277316.

Rocha, C. B., S. T. Gille, T. K. Chereskin, and D. Menemenlis, 2016: Seasonality of submesoscale dynamics in the Kuroshio Extension. *Geophysical Research Letters*, **43 (21)**, 11,304–11,311, https://doi.org/10.1002/2016GL071349.

Rosso, I., A. M. Hogg, A. E. Kiss, and B. Gayen, 2015: Topographic influence on submesoscale dynamics in the Southern Ocean. *Geophysical Research Letters*, **42 (4)**, 1139–1147, https://doi.org/10.1002/2014GL062720.

Ruiz, S., A. Pascual, B. Garau, I. Pujol, and J. Tintoré, 2009: Vertical motion in the upper ocean from glider and altimetry data. *Geophysical Research Letters*, **36 (14)**, https://doi.org/10.1029/2009GL038569.

Sallée, J.-B., R. J. Matear, S. R. Rintoul, and A. Lenton, 2012: Localized subduction of anthropogenic carbon dioxide in the Southern Hemisphere oceans. *Nature Geoscience*, **5 (8)**, 579–584, https://doi.org/10.1038/ngeo1523.

Sallée, J.-B., and Coauthors, 2021: Summertime increases in upper-ocean stratification and mixed-layer depth. *Nature*, **591 (7851)**, 592–598, https://doi.org/10.1038/s41586-021-03303-x.

Shi, J.-R., L. D. Talley, S.-P. Xie, Q. Peng, and W. Liu, 2021: Ocean warming and accelerating Southern Ocean zonal flow. *Nature Climate Change*, **11 (12)**, 1090–1097, https://doi.org/10.1038/s41558-021-01212-5.

Siegelman, L., 2020: Energetic Submesoscale Dynamics in the Ocean Interior. *Journal of Physical Oceanography*, **50 (3)**, 727–749, https://doi.org/10.1175/JPO-D-19-0253.1.

Siegelman, L., P. Klein, P. Rivière, A. F. Thompson, H. S. Torres, M. Flexas, and D. Menemenlis, 2020: Enhanced upward heat transport at deep submesoscale ocean fronts. *Nature Geoscience*, **13 (1)**, 50–55, https://doi.org/10.1038/s41561-019-0489-1.

Simoes-Sousa, I. T., A. Tandon, F. Pereira, C. Z. Lazaneo, and A. Mahadevan, 2022: Mixed layer eddies supply nutrients to enhance the spring phytoplankton bloom. *Frontiers in Marine Science*, **9**, https://doi.org/10.3389/fmars.2022.825027.

Smith, K. M., P. E. Hamlington, and B. Fox-Kemper, 2016: Effects of submesoscale turbulence on ocean tracers. *Journal of Geophysical Research: Oceans*, **121 (1)**, 908–933, https://doi.org/https://doi.org/10.1002/2015JC011089.

Sokolov, S., and S. R. Rintoul, 2007: Multiple Jets of the Antarctic Circumpolar Current South of Australia. *Journal of Physical Oceanography*, **37 (5)**, 1394–1412, https://doi.org/10.1175/JPO3111.1.

Somavilla, R., C. González-Pola, and J. Fernández-Diaz, 2017: The warmer the ocean surface, the shallower the mixed layer. How much of this is true? *Journal of Geophysical Research: Oceans*, **122 (9)**, 7698–7716, https://doi.org/10.1002/2017JC013125.

Spall, M. A., 1995: Frontogenesis, subduction, and cross-front exchange at upper ocean fronts. *Journal of Geophysical Research: Oceans*, **100 (C2)**, 2543–2557, https://doi.org/10.1029/94JC02860.

Stamper, M. A., J. R. Taylor, and B. Fox-Kemper, 2018: The Growth and Saturation of Submesoscale Instabilities in the Presence of a Barotropic Jet. *Journal of Physical Oceanography*, **48 (11)**, 2779–2797, https://doi.org/10.1175/JPO-D-18-0022.1.

Stewart, K. D., and T. W. N. Haine, 2016: Thermobaricity in the Transition Zones between Alpha and Beta Oceans. *Journal of Physical Oceanography*, **46 (6)**, 1805–1821, https://doi.org/10.1175/JPO-D-16-0017.1.

Su, Z., J. Wang, P. Klein, A. F. Thompson, and D. Menemenlis, 2018: Ocean submesoscales as a key component of the global heat budget. *Nature Communications*, **9 (1)**, 775, https://doi.org/10.1038/s41467-018-02983-w.

Sverdrup, H. U., 1953: On Conditions for the Vernal Blooming of Phytoplankton. *ICES Journal of Marine Science*, **18**, 287–295, https://doi.org/10.1093/icesjms/18.3.287.

Tamsitt, V., and Coauthors, 2017: Spiraling pathways of global deep waters to the surface of the Southern Ocean. *Nature Communications*, **8 (1)**, 1–10, https://doi.org/10.1038/s41467-017-00197-0.

Taylor, J. R., and A. F. Thompson, 2023: Submesoscale Dynamics in the Upper Ocean. *Annual Review of Fluid Mechanics*, **55 (1)**, null, https://doi.org/10.1146/annurev-fluid-031422-095147.

Thomas, L. N., 2008: Formation of intrathermocline eddies at ocean fronts by wind-driven destruction of potential vorticity. *Dynamics of Atmospheres and Oceans*, **45 (3)**, 252–273, https://doi.org/10.1016/j.dynatmoce.2008.02.002.

Thomas, L. N., A. Tandon, and A. Mahadevan, 2013: Submesoscale Processes and Dynamics. *Ocean Modeling in an Eddying Regime*, American Geophysical Union (AGU), 17–38, URL https://agupubs.onlinelibrary.wiley.com/doi/abs/10.1029/177GM04.

Thompson, A. F., and A. C. Naveira Garabato, 2014: Equilibration of the Antarctic Circumpolar Current by Standing Meanders. *Journal of Physical Oceanography*, **44 (7)**, 1811–1828, https://doi.org/10.1175/JPO-D-13-0163.1.

Treguier, A. M., and Coauthors, 2023: The mixed-layer depth in the Ocean Model Intercomparison Project (OMIP): impact of resolving mesoscale eddies. *Geoscientific Model Development*, **16 (13)**, 3849–3872, https://doi.org/10.5194/gmd-16-3849-2023.

Uchida, T., D. Balwada, R. P. Abernathey, G. McKinley, S. Smith, and M. Lévy, 2019: The Contribution of Submesoscale over Mesoscale Eddy Iron Transport in the Open Southern Ocean.

Journal of Advances in Modeling Earth Systems, **11 (12)**, 3934–3958, https://doi.org/10.1029/2019MS001805.

Vic, C., J. Gula, G. Roullet, and F. Pradillon, 2018: Dispersion of deep-sea hydrothermal vent effluents and larvae by submesoscale and tidal currents. *Deep Sea Research Part I: Oceanographic Research Papers*, **133**, 1–18, https://doi.org/10.1016/j.dsr.2018.01.001.

Wang, S., and Coauthors, 2022: Weakened Submesoscale Eddies in the Equatorial Pacific Under Greenhouse Warming. *Geophysical Research Letters*, **49 (21)**, e2022GL100 533, https://doi.org/10.1029/2022GL100533.

Yamaguchi, R., and T. Suga, 2019: Trend and Variability in Global Upper-Ocean Stratification Since the 1960s. *Journal of Geophysical Research: Oceans*, **124 (12)**, 8933–8948, https://doi.org/10.1029/2019JC015439.

Yu, X., A. C. N. Garabato, A. P. Martin, C. E. Buckingham, L. Brannigan, and Z. Su, 2019: An Annual Cycle of Submesoscale Vertical Flow and Restratification in the Upper Ocean. https://doi.org/10.1175/JPO-D-18-0253.1.

Yung, C. K., A. K. Morrison, and A. M. Hogg, 2022: Topographic Hotspots of Southern Ocean Eddy Upwelling. *Frontiers in Marine Science*, **9**, https://doi.org/10.3389/fmars.2022.855785.

Zhang, Y., D. Chambers, and X. Liang, 2021: Regional Trends in Southern Ocean Eddy Kinetic Energy. *Journal of Geophysical Research: Oceans*, **126 (6)**, e2020JC016 973, https://doi.org/10.1029/2020JC016973.

Supplemental Information: Pycnocline Stratification Shapes Submesoscale Vertical Tracer Transport

Lilian A. Dove[a,b] , Mara A. Freilich[a] , Lia Siegelman[c] , Baylor Fox-Kemper[a] , Paul Hall[a]

[a] *Brown University, Providence, Rhode Island, USA,* [b] *Cooperative Programs for the Advancement of Earth System Science, University Corporation for Atmospheric Research, Boulder, Colorado, USA,* [c] *Scripps Institution of Oceanography, La Jolla, California, USA*

Corresponding author: Lily Dove, dove@brown.edu

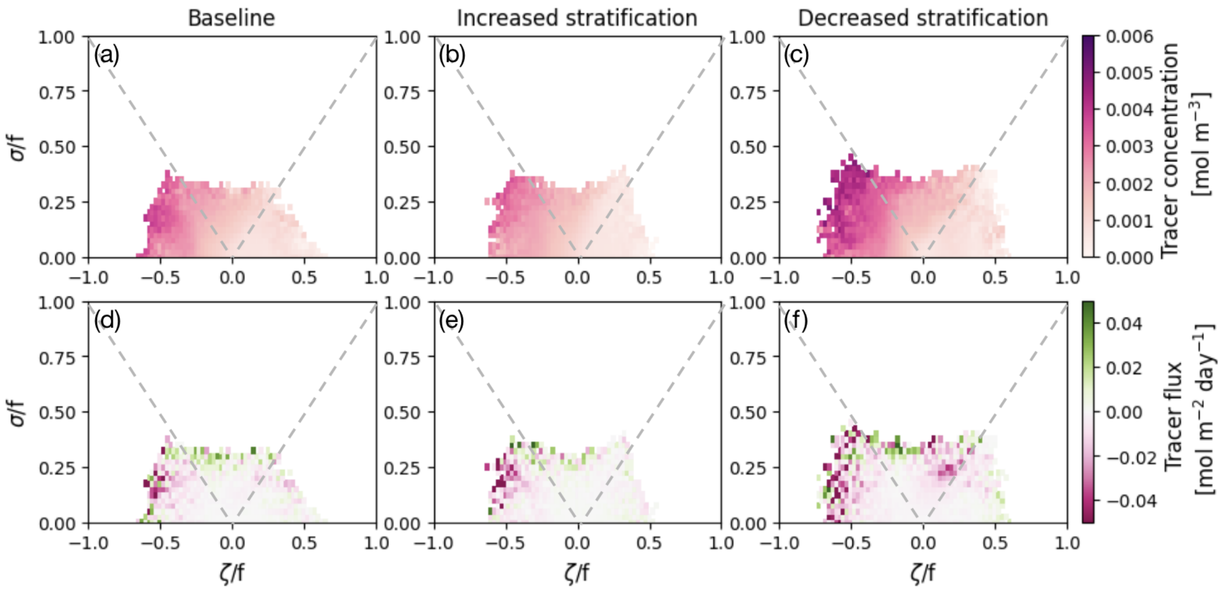

FIG. 1. Joint histograms of Rossby number (ζ/f) and strain (σ/f) at 350 m with a *changing isopycnal slope*. Colored by (a),(c),(e) average tracer concentration [mol m^{-3}] and (b),(d),(f) average tracer flux [mol m^{-2} day^{-1}] per ζ and σ pair. For flux, negative values indicate downwards flux. ζ and σ pairs with fewer than 10 points were disincluded for averaging purposes.

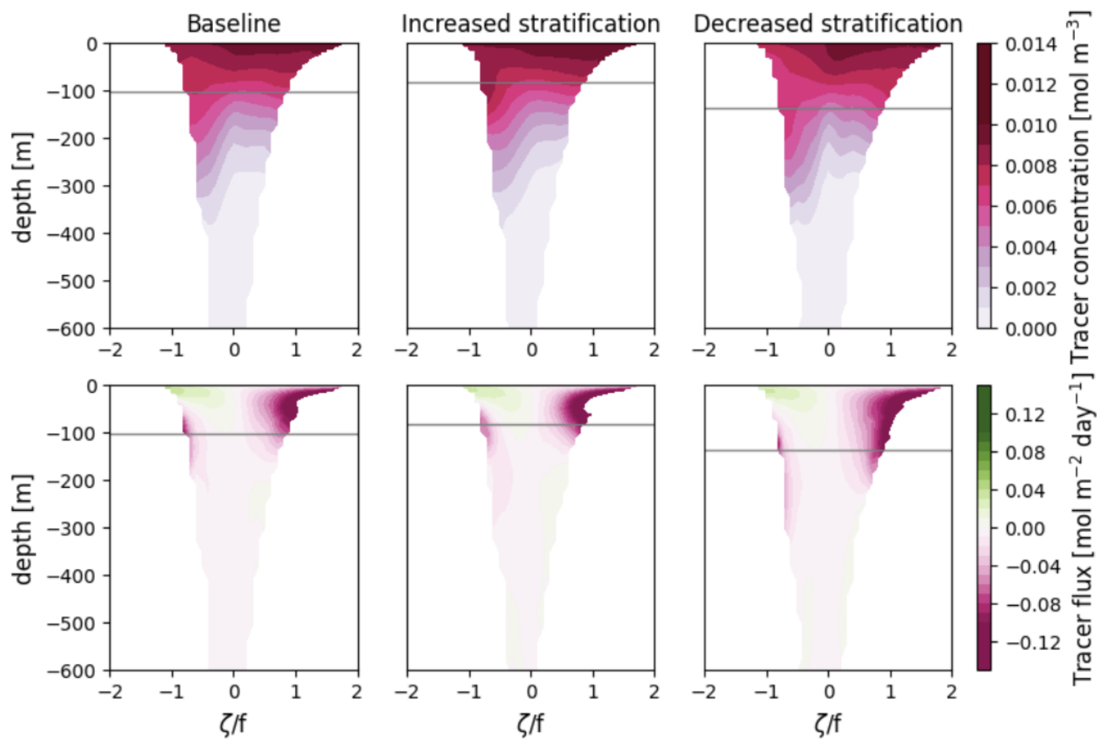

FIG. 2. Tracer concentration and tracer flux over depth with a *changing isopycnal slope*. Colored by (a)-(c) average tracer concentration [mol m^{-3}] per Rossby number (ζ/f), weighted by area covered by that Rossby number at that depth. (d)-(f) average tracer flux [mol m^{-2} day^{-1}] per ζ/f. Gray lines represent the average mixed layer depth for each stratification case.

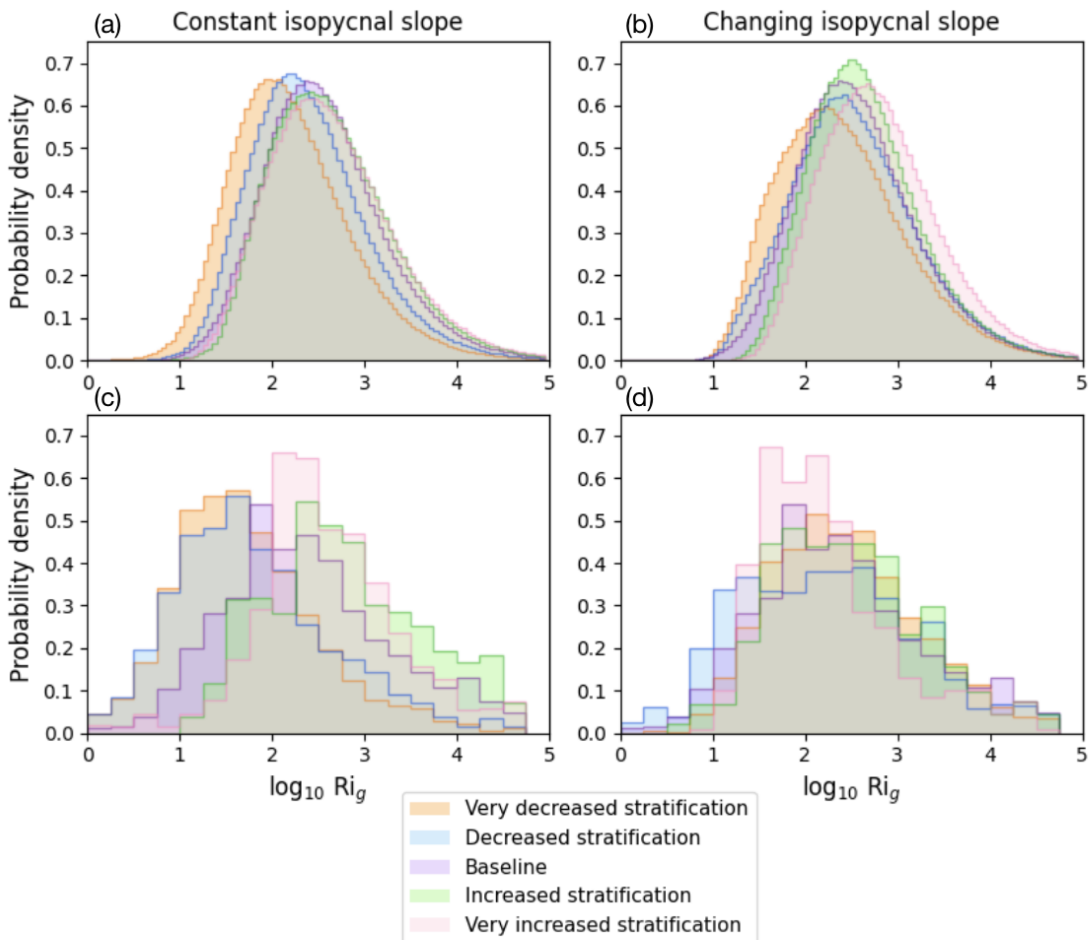

FIG. 3. Probability density functions of Ri_g at 350 m. Full distribution for (a) constant isopycnal slope and (b) changing isopycnal slope conditions. Just points with Ro < -0.5 for (c) constant isopycnal slope and (d) changing isopycnal slope conditions.